

**DESIGN, OPTIMIZATION AND IMPLEMENTATION OF  
AN ORTHO-TAG RFID SYSTEM**

by

**Xiaoyu Liu**

BS in Electrical Engineering, Tsinghua University, 2005

MS in Electrical Engineering, Tsinghua University, 2007

Submitted to the Graduate Faculty of  
the Swanson School of Engineering in partial fulfillment  
of the requirements for the degree of  
Doctor of Philosophy

University of Pittsburgh

2011

UNIVERSITY OF PITTSBURGH  
SWANSON SCHOOL OF ENGINEERING

This dissertation was presented

by

Xiaoyu Liu

It was defended on

October 07, 2011

and approved by

Marlin H. Mickle, PhD, Nickolas A. DeCecco Professor, Department of Electrical and  
Computer Engineering

Mingui Sun, PhD, Professor, Department of Neurological Surgery, Department of Electrical  
and Computer Engineering

Zhi-Hong Mao, PhD, Associate Professor, Department of Electrical and Computer  
Engineering

James T. Cain, PhD, Professor Emeritus, Department of Electrical and Computer Engineering

George Stetten, MD, PhD, Professor, Department of Bioengineering

Dissertation Director: Marlin H. Mickle, PhD, Nickolas A. DeCecco Professor, Department  
of Electrical and Computer Engineering

Copyright © by Xiaoyu Liu

2011

**DESIGN, OPTIMIZATION AND IMPLEMENTATION OF  
AN ORTHO-TAG RFID SYSTEM**

Xiaoyu Liu, PhD

University of Pittsburgh, 2011

There are two major problems with traditional methods of operating an RFID tag embedded on orthopedic implants by wireless transmission: (1) interference with metallic orthopedic implants causes significant signal attenuation around the RFID tag; (2) interference with other medical devices may lead to the failure of their functionality. The creation of a feasible solution to the above two problems is critical to the success of operation of implanted RFID devices embedded on or near metallic implants and in any other situation where wireless interference may occur. The solution proposed in this dissertation is the Ortho-tag RFID system which uses the conductivity of human tissue at radio frequencies for energy and signal transmission. With the viability experiments proving the feasibility of using volume conduction in this research, two present issues have been addressed: (1) the lack of availability of a matching technique between tissue/saline and the RFID device; (2) the lack of an efficiency study on the operation of RFID through tissue/saline with variable thickness. This fundamental work then details the development of a general solution for the above two issues, in a power and communication platform technology for implanted RFID devices. The platform is developed using equipment in the RFID Center of Excellence in which pig skin and saline are used as a medium for *in vivo* environment as human tissue surrogates. The selection and design of the volume conduction electrodes are discussed and optimized using ANSYS/HFSS. The system optimization focuses on matching the RFID reader and the tag to the tissue/saline based on an equivalent 2-port

network model for tissue using  $Z$  parameters. Matching networks are designed and optimized so that the tag is matched to the tissue from the internal side, and the tissue is matched to the RFID reader from the external side. For high data rate considerations, two RFID frequencies are utilized for the Ortho-tag RFID system. The frequencies are HF at 13.56 MHz and UHF at 915 MHz. The system is finally prototyped and demonstrated as the proof of concept.

**Keywords:** RFID, volume conduction, Ortho-tag, orthopedic implant, matching

## TABLE OF CONTENTS

<b>PREFACE.....</b>	<b>XIV</b>
<b>1.0 INTRODUCTION.....</b>	<b>1</b>
<b>1.1 DEMANDS FOR SMART ORTHOPEDIC IMPLANTS.....</b>	<b>3</b>
<b>1.2 STATEMENT OF PROBLEM .....</b>	<b>4</b>
<b>1.3 DISSERTATION OUTLINE.....</b>	<b>7</b>
<b>2.0 BACKGROUND AND PRILIMINARY STUDY .....</b>	<b>8</b>
<b>2.1 RFID SYSTEM AND TECHNOLOGY .....</b>	<b>8</b>
<b>2.1.1 HF RFID system .....</b>	<b>11</b>
<b>2.1.2 UHF RFID system .....</b>	<b>12</b>
<b>2.2 PROBLEMS WITH EXISTING SYSTEMS .....</b>	<b>13</b>
<b>2.2.1 Metallic interference.....</b>	<b>13</b>
<b>2.2.2 Signal attenuation through tissue.....</b>	<b>16</b>
<b>2.3 VOLUME CONDUCTION.....</b>	<b>16</b>
<b>2.3.1 System architecture .....</b>	<b>17</b>
<b>2.3.2 Electrodes patterns .....</b>	<b>18</b>
<b>2.3.3 Matching networks.....</b>	<b>20</b>
<b>2.4 VOLUME CONDUCTION BASED RFID SYSTEM.....</b>	<b>21</b>
<b>2.5 PRILIMINARY STUDIES .....</b>	<b>22</b>

2.5.1	The saline container.....	23
2.5.2	Electrodes in experiments.....	24
2.5.3	Signal attenuation.....	25
2.5.4	Experimental demonstration.....	27
<b>3.0</b>	<b>SYSTEM DESIGN.....</b>	<b>30</b>
3.1	PROPOSED ORTHO-TAG RFID SYSTEM.....	30
3.2	TOUCH PROBE.....	32
3.2.1	Structure of the touch probe.....	32
3.2.2	Matching network for the touch probe.....	35
3.3	ORTHO-TAG.....	36
3.3.1	Electrode design.....	36
3.3.2	Matching network for the Ortho-tag.....	38
3.3.3	Electrode material.....	39
3.4	RFID READER CONFIGURATION.....	40
3.5	SOFTWARE DESIGN.....	41
<b>4.0</b>	<b>SYSTEM OPTIMIZATION.....</b>	<b>45</b>
4.1	DESIGN TOOL.....	45
4.2	THE TISSUE MODEL.....	48
4.3	HF SYSTEM OPTIMIZATION.....	51
4.3.1	The electrode optimization.....	51
4.3.1.1	The objective function.....	52
4.3.1.2	Optimization methodology.....	54
4.3.2	Matching network optimization.....	55

4.3.2.1	Impedance calculation .....	55
4.3.2.2	LC value calculation .....	58
4.4	UHF SYSTEM OPTIMIZATION.....	59
4.4.1	UHF touch probe optimization.....	59
4.4.2	UHF Ortho-tag optimization .....	62
4.5	THE DESIGN FLOW .....	64
5.0	PROTOTYPE AND VERIFICATION .....	66
5.1	HF ORTHO-TAG RFID SYSTEM.....	66
5.2	UHF ORTHO-TAG RFID SYSTEM.....	69
5.3	ERROR ANALYSIS.....	72
5.3.1	Electrode-skin interface impedance.....	72
5.3.2	Temperature and humidity.....	73
5.3.3	Other factors .....	74
6.0	DISCUSSIONS .....	76
6.1	POWER VS TAG SIZE .....	76
6.1.1	HF Ortho-tag size .....	77
6.1.2	UHF Ortho-tag size .....	79
6.2	THE POWER VS ANGLE .....	80
6.3	HF SYSTEM VS UHF SYSTEM .....	83
7.0	CONTRIBUTION OF WORK .....	87
8.0	CONCLUSION.....	88
APPENDIX A. VARIABLES DEFINED IN HFSS SIMULATION .....		89
APPENDIX B. MATLAB CODE FOR ELECTRODE OPTIMIZATION.....		90

<b>APPENDIX C. MATLAB CODE FOR LOAD IMPEDANCE OPTIMIZATION .....</b>	<b>93</b>
<b>APPENDIX D. MATLAB CODE FOR CALCULATING MATCHING NETWORK PARAMETERS FOR THE HF ORTHO-TAG .....</b>	<b>95</b>
<b>APPENDIX E. MATLAB CODE TO GENERATE THE MATCHING CHART FOR THE UHF SYSTEM.....</b>	<b>97</b>
<b>APPENDIX F. MATLAB CODE FOR PLOTTING TAG SIZE VS POWER.....</b>	<b>99</b>
<b>APPENDIX G. MATLAB CODE FOR PLOTTING TAG ANGLE VS POWER.....</b>	<b>102</b>
<b>BIBLIOGRAPHY.....</b>	<b>104</b>

## LIST OF TABLES

Table 1. Impedance from simulation and measurements for the HF system.....	68
Table 2. Reading range for the HF system .....	69
Table 3. Impedance from simulation and measurements for the UHF system.....	70
Table 4. Reading range for the UHF system.....	71
Table 5. Voltage efficiency with different placement of touch probe .....	82

## LIST OF FIGURES

Figure 1. A typical RFID system .....	9
Figure 2. The Magellan HF RFID system .....	12
Figure 3. The SAMSys UHF RFID system .....	13
Figure 4. Test configurations for RFID metallic interference using wireless way.....	15
Figure 5. A typical volume conduction system .....	18
Figure 6. Existing patterns of electrodes.....	19
Figure 7. The optimized electrode design in the existing literature.....	19
Figure 8. The saline container for signal attenuation measurement .....	24
Figure 9. Round electrodes with variable sizes .....	24
Figure 10. Signal attenuation measurement results. ....	26
Figure 11. The original version of implanted Ortho-tag.....	28
Figure 12. Reading the Ortho-tag through saline and pig skin.....	28
Figure 13. The proposed Ortho-tag RFID system. ....	31
Figure 14. Diagram of the HF touch probe.....	33
Figure 15. Diagram of the UHF touch probe.....	34
Figure 16. Equivalent circuit model of the matching network for the touch probe.....	35
Figure 17. Diagram of the Ortho-tag .....	36

Figure 18. Equivalent circuit model of the matching network for Ortho-tag .....	38
Figure 19. Signal being sent after reader is powered on .....	40
Figure 20: A cycle of operating the reader through PC .....	42
Figure 21. Flow chart for the read operation .....	43
Figure 22. Test of the software design.....	44
Figure 23. The patient registry.....	44
Figure 24. The knee implant model in HFSS .....	47
Figure 25. The simulated electrical field distribution in tissue.....	47
Figure 26. Modeling the tissue as a two port network.....	49
Figure 27. Proposed Ortho-tag electrodes .....	53
Figure 28. Creation of the inner border of electrodes.....	53
Figure 29. Touch probe impedance changes vs. $C_s$ and $C_p$ .....	61
Figure 30. The matching chart for the UHF touch probe .....	61
Figure 31. The control parameters for the UHF matching network .....	63
Figure 32. UHF Ortho-tag impedance changes vs. $s$ and $D_1$ .....	63
Figure 33. UHF Ortho-tag matching chart.....	64
Figure 34. The design flow for optimizing the Ortho-tag RFID system .....	65
Figure 35. The prototype HF touch probe and HF Ortho-tag.....	67
Figure 36. The prototype UHF touch probe and UHF Ortho-tag.....	70
Figure 37. Experiment on a UHF system using pig skin with a knee implant .....	71
Figure 38. Power vs. tag size for HF Ortho-tag.....	77
Figure 39. The 3D plot for the relationship between power and HF tag dimension.....	78
Figure 40. Power vs. tag size for UHF Ortho-tag.....	79

Figure 41. The 3D plot for the relationship between power and UHF tag dimension..... 80

Figure 42. The different placements of the touch probe..... 81

Figure 43. Touch probe placement vs. efficiency for HF and UHF systems..... 83

## **PREFACE**

Many people have said that a PhD degree is one of the most difficult jobs to finish, not only because of its long duration, but also the uncertainty of the research results. However, you can never tell before you get it. As for me, this is a process I must undergo before I grow as a scientist and a professional. I encountered happiness when experiments were as expected, and of course, I had my hard time when everything was frustrating. I once even doubted if this research was worth doing. But finally, after overcoming many difficulties, I say proudly that this work will be one of the most exciting and meaningful things in my life.

I must thank my parents first, who have always encouraged and supported me through their love and an unspoken pride. Their firm stand behind me gave me courage when I was depressed. Without their support, I could not even come to the US to start my PhD study.

Of course, I must thank my advisor, Dr. Mickle, for the opportunity to work in his laboratory. He usually tells stories, from which I feel that he has pushed me in such a way to challenge me for the better. Through his guidance and encouragement, I always have a faith of success in my mind and have overcome many difficulties during this tough period and later grown as a competent scientist in research. I must also thank Dr. Sun, Dr. Mao, Dr. Cain and Dr. Stetten for their kind support and commentary during my PhD study, which always provides a transparent view of the world which led me to new discoveries.

I must also thank Dr. Minhong Mi and Dr. Vogel from ANSYS Inc, who gave me kind support on the simulation part of my dissertation using HFSS. I must thank Dr. Berger too, for the opportunity of my dissertation topic and support of the orthopedic implants.

My labmates, both past and present, have also played important roles both in my course work and research. Through working and discussion with them, I have gained a lot of experience by thinking from different aspects of view. Without their help, discussion and friendship, the journey for my PhD study would be much more difficult.

Finally, and not least of all, I would like to show my appreciation for the financial support from University of Pittsburgh during my PhD study and this research. Thanks to Dr. Mickle, Dr. Berger and the Office of Technology Management.

## 1.0 INTRODUCTION

Orthopedic implants are medical devices used to replace or provide fixation of bone or to replace the articulating surfaces of a joint. Nowadays they are widely incorporated in clinical applications for people who have severe joint diseases such as osteoarthritis - a disease causing cartilage to wear down resulting in painful bone to bone contact [1]. By replacing the old joint with a new artificial one, orthopedic implants do not only give back quality of life but also help in increasing mobility and reducing pain.

As the utilization of orthopedic surgeries becomes common, some inconvenient aspects have occurred which require improvements from both patients and surgeons. One of the urgent problems to solve is the difficulty in identifying the orthopedic implants once they have been implanted, because the current methods for obtaining such information are not efficient: paper based records add difficulty in keeping and tracking, as well as increasing the risk of counterfeiting and mistakes during manually information input; computer based database are not easy to access by one hospital from another hospital because of privacy concerns, let alone they are not always achievable. Another problem is the difficulty in monitoring the status of the orthopedic implants, such as pressure and position, which is of great important during the recovery stage. The current method used is taking an X-ray picture for surgeons to diagnose how well the implants fit in the body. However, besides its cost and time, sometimes, it is impossible to obtain the overall information to judge the status of the implants from only a few pictures.

Based on the above two urgent requirements for the orthopedic implants, a new concept named “smart implant” has been proposed [2] [3]. From its name, a smart implant should have two abilities: (1) ease in identification and tracking; (2) ease for status monitoring.

For the tracking and identification capabilities, by comparing possible solutions, an RFID (Radio Frequency Identification) tag will be among the best. An RFID tag is a transponder equipped with an antenna and a chip for information and communication. RFID tags are widely used in the real world today for identifying products using tags for everyday commodities such as the Wal-mart tags to tags for aircraft components [4] [5] and even to hospital applications [6]. In this work, the RFID tag embedded on an orthopedic implant for identification and monitoring purposes is defined as an “Ortho-tag”. The information of the orthopedic implant such as the basic product information, as well as other related information can be stored on the Ortho-tag, for identification purposes. The Ortho-tag can also be communicating with bio-sensors placed around the implant for monitoring the status of the implant.

Throughout the literature on RFID systems, especially the design of tags, numerous designs hold great potential. However, among the existing tags, most of them are designed for use in a specific environment or a specific operational case, meaning that a tremendous decrease in efficiency may possibly occur if environment changes. Therefore, despite the variety of tag designs in the market, none of them is suitable for working with an orthopedic implant. The main reason includes the operation environment for the tag is with both the biological tissue and the metal implant, a complex environment that never has been successfully studied for an RFID tag. In this work, a new method of operating an implanted RFID tag using volume conduction is proposed, termed the Ortho-tag RFID system, to work in such an environment on orthopedic implants. The two significant problems which continue to impede the widespread utilization of

the Ortho-tag RFID type systems are (1) the lack of availability of an energy efficient transmission strategy for the pattern of the Ortho-tag and (2) the lack of a matching technology to impedance match the tag in low power conditions. The research described in this work addresses these issues, focusing on the design of a specific system as a proof-of-concept application of the technology.

## **1.1 DEMANDS FOR SMART ORTHOPEDIC IMPLANTS**

As the advancement of the quality of orthopedic surgeries guarantees satisfaction for patients who have severe joint problems, there has been an increasing demand for the orthopedic implants in the recent years by a report of the American Academy of Orthopedic Surgeons (AAOS) [7] in 2006. Detailed information shows the total number of knee and hip replacement surgeries keeps increasing from the year 2000 to 2005, and especially, in the year 2005, a total number of 750, 000 hip and knee prostheses were implanted in the US, representing a 70 percent increase from the previous 5 years [8]. In addition, such demands will keep increasing as the population ages. By the year 2030, it is estimated that the number of knee replacements will increase 6-fold from 450,400 to an approximate total of 3.48 million, a 673 percent increase in total-knee replacements and a 174 percent increase in first-time total-hip replacements.

From the business side, a recent study by a market research group shows that the size of the market for orthopedic implants will undergo a rapid annual increase of 8.9%, which can be attributed to baby boomers, more active lifestyles, and advances in technologies. It is reported that the strong demand for orthopedic implants will push the market's growth to almost \$22 billion by 2012, after analyzing the \$14.3 billion US orthopedic implant industry in 2007 [9].

However, as the market is growing, periprosthetic infection caused by deep tissue infection will also rise as the increase of joint replacement surgeries increases. According to reports in 2005 and 2007, it has been estimated to occur in between 1% and 4% of surgeries and is projected to increase between 2005 and 2030 by nearly 14-fold, from 3400 cases to 46,000 cases, for total hip replacement and by approximately 27-fold, from 6,400 cases to 175,500 cases, for total knee replacement [10] [11]. With the growing demand for both original hip and knee replacements, along with the attendant need for implant revisions, there will also be an increasing need to monitor the condition of the implant and biological environment in which it exists without using invasive procedures. Besides all the above, with the rapid increase in the number of implants to be used in treating hip and knee joints, manufacturers are increasingly concerned over the production of counterfeit devices sold under the same name as the legitimate one. As a result, the growing market for the orthopedic implants expedites the growing demand for smart orthopedic implants, forming a huge potential market in the near future.

## **1.2 STATEMENT OF PROBLEM**

Because there is no existing report of RFID device embedded on orthopedic implants either in experimental trial or industry application, the principle work of this dissertation is to design and optimize an Ortho-tag RFID system that can be embedded on an orthopedic implant for implant identification. Several issues will be discussed and addressed in this dissertation regarding developing an efficient energy transmission platform for the Ortho-tag RFID system. These problems include the well-known interference between the RF signal and the orthopedic implant,

lack of matching technique that matches the Ortho-tag system to both implant and human tissue and concerns over the alignment of the Ortho-tag devices including the touch probe and tag alignment. First, the RF interference with the implant tremendously degrades the field strength along its transmitting path, preventing the RFID device from receiving enough operating power. To solve this problem, a non-conventional wireless energy transmission technology, named volume conduction [39], a technology, which relies on conductivity of tissue for power transmission to avoid metallic interference, will be utilized in combination with the existing RFID technology as the Ortho-tag RFID system energy transmission platform. Another issue then becomes the optimization of the proposed volume conduction based RFID system for maximizing efficiency by means of optimizing the volume conduction electrodes in their shape and size and the matching networks. Because of the lack of a matching technology in the reported literature that can match an RFID device to metal and tissue, a methodology in optimizing the Ortho-tag system through matching is extremely important as its significant impact on efficiency. To address this issue, methods of designing the matching network and optimizing electrodes based on the  $Z$  matrix of classical circuit theory [64] obtained from ANSYS/HFSS simulation will be developed in this dissertation for the HF (13.56MHz) Ortho-tag system. A method of designing matching network using meander line inductors will be developed for the UHF Ortho-tag system with matching charts obtained from HFSS. Concerns over the tag size and the touch probe placement are also important in that they are closely related along with how much power the Ortho-tag can receive. With the Ortho-tag system being optimized, further discussion on concerns with the touch probe alignment and tag size selection in respect to the power efficiency will be detailed after a number of simulations with different

alignment cases and tag sizes have been performed, and a graphic interpretation will also be created from HFSS as the reference for understanding.

In summary, the dissertation work includes:

- Establish the overall framework to integrate commercially available RFID chips and readers into a functional system overcoming the problems of operation in a metallic environment and a non-air, i.e., tissue medium
- Develop an empirical methodology to verify engineering modeling through an empirical in-vivo testing environment
- Design a customized RFID tag by integrating a commercial RFID chip with matching circuitry with electrodes for harvesting energy and communicating with an RFID reader
- Derive the scientific basis to match the electrodes of the tag to the air medium antenna inputs of the commercial RFID chip to a tissue medium
- Derive the scientific basis to match connecting electrodes to a commercial RFID reader to a tissue medium
- Derive the mathematical basis to model and optimize the matching problem for both the reader and chip
- Using the framework established, set up testing procedures to verify the designs and methodologies for electrodes and matching
- Conduct the testing and analysis to verify the ability to operate a commercial air medium RFID system as a commercial viable tissue medium RFID system
- Analyze the relationship between the size of tag and power and the relationship between location of the touch probe and power transmission efficiency through tissue medium

### **1.3 DISSERTATION OUTLINE**

This dissertation is presented in six main sections. The first section discusses the background for the Ortho-tag system, including the RFID technology, volume conduction technology and related work. Some preliminary results from this dissertation to demonstrate the feasibility of the proposed method are also introduced and discussed. These topics are important foundational work from which to build and compare the Ortho-tag RFID system and model. The second section introduces the background of this dissertation with preliminary work as a support. The third section of the dissertation details the Ortho-tag that has been built and the overall system for which it is used. Following is the fourth section, which details how matching has been implemented to the Ortho-tag and the touch probe. Prototype and verification of the Ortho-tag system are covered in the fifth section with measured data for studying system performance. The sixth section mainly discusses about the size considerations of the Ortho-tag with proposed methods to miniaturize the tag for practical uses as well as briefly followed by the general conclusions of the work.

## **2.0 BACKGROUND AND PRILIMINARY STUDY**

This chapter describes the fundamental knowledge and techniques to be applied for the Ortho-tag RFID system. This knowledge and sort of techniques include the introduction of typical RFID system and it technology and discussion on current problems for orthopedic implants using existing RFID systems and the volume conduction technology. The introduction of the RFID system focuses on the review of the system construction with details on its components, applications and operations. Two major issues using current RFID systems on orthopedic implants are brought forward and discussed which leads to the solution proposed in this work – the volume conduction technology. In order to address the problems with existing operation of RFID systems, a novel Ortho-tag RFID system is proposed which incorporates the RFID system with volume conduction technology to promote the energy transmission efficiency when attached to an orthopedic implant. The last section of this chapter leads to the preliminary studies and experiments on the Ortho-tag RFID system which demonstrates the feasibility of this new technology with further discussion on its clinical applications in the near future.

### **2.1 RFID SYSTEM AND TECHNOLOGY**

Radio frequency identification (RFID) technology is a data communication technology using radio frequency waves for information exchange between a terminal and an object [12]. The

system involves interrogators (readers) and tags (figure 1). The tag is a transponder consisting of an antenna and an IC chip to receive a specific signal and automatically transmit a specific reply through a wireless link. The main blocks of the chip include a front end analog circuitry for modulating and demodulating signals into and from the radiofrequency wave format, a digital logic to control each block and process commands, and an erasable memory for information storage. The information can be as simple as a single ID number or can be more detailed data such as manufacturer and distributor information depending on the size of memory and time allowed to obtain the data. Due to its highly integrated design, the tag can be made small in size and usually consumes a very low power. Based on the powering ability, there are mainly three types of RFID tags. Active tags are those ones operated by a designated battery with their own transmitting capability independent of the reader; passive tags are those without a battery and being powered purely by the energy captured from the electromagnetic field with its communication depending on reflected signal; semi-passive tags are between the two: they have a battery only for the tag electronics but not for transmitting radio [13]. A specially designed rectifier and a regulator are included in the front end circuitry of a passive tag as the captured electromagnetic energy needs to be converted into regulated DC power so as to power the remaining parts of the tag [14].

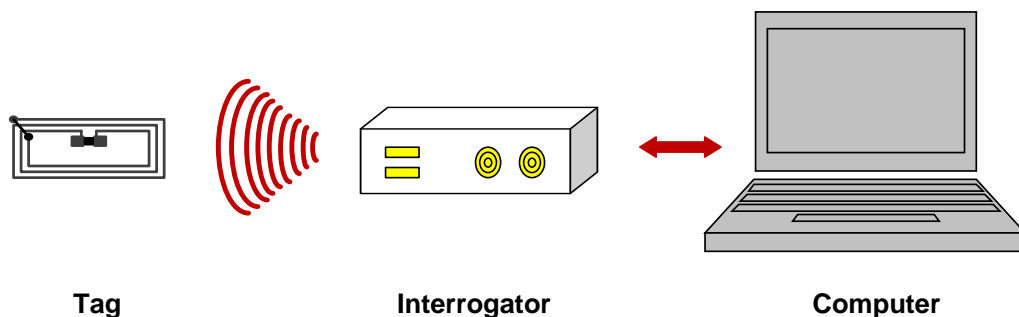


**Figure 1.** A typical RFID system

Upon receiving a wake-up signal from the reader, the tag first comes into a power mode with its chip being turned on and waiting. If the reader sends a request to the tag, the tag then updates its state machine with corresponding memory operations and then backscatters a response. The memory size of the tag is usually from bytes to kilobytes, up to 32 kilobytes by current technology [15], which is sufficient for both essential information like a product tracking ID in the Wal-mart tags and extended information such as the patient registry to be written in an Ortho-tag. Because of its readable and writable features, RFID tags were first invented to be attached to products or product packages for identification and tracking purposes to reduce the time and error in logistics [16]. Fast response RFID tags are also installed in vehicles for identification and monitoring purposes as in the road toll system or parking system [17]. Furthermore, the objects to be tracked by an RFID system can also be alive, like animals or even humans, which have been proposed and experimentally realized [18, 19, 20].

Passive tags, due to their operation without batteries, are more popular in systems where the longevity of use is principle and range of operation does not need to be long. The ranges of passive tags are usually less than ten meters in power transmission because of the weak RF field at far end. Because battery is a major concern for any implantable devices, as replacing batteries is extremely expensive, passive tags are preferred when embedding on orthopedic implants. Additionally, there are also several advantages in using passive tags for the orthopedic implants. First, they are low in cost: the cost is only several cents per tag for mass production. Second, they are more flexible in design as the elimination of concerns for battery connection. Third, advancements in technology in tags guarantee the availability of reliable and long-lasting passive tags in the market.

There are different protocols and compliances regulating the manufacturing of passive tags for different operating frequencies. Standard operating frequencies range from low frequency (LF) to ultra high frequency (UHF). Low frequency RFID systems were common in the past, when high frequency systems were hard to implement. However, to obtain fast data rate and the capability to operate multiple tags at one time, HF and UHF systems are widely used presently. The six common operating frequencies for RFID systems in United States are 125 KHz, 134.2 KHz, 13.56 MHz, 433 MHz, 915 MHz and 2.45GHz among which 13.56MHz and 915MHz are widely used and typically designated for passive RFID systems. Generally speaking, if using the same modulation, the higher the frequency is, the higher the data rate that can be achieved because the time interval between each data symbol becomes smaller [21]. However, the data rate in some HF RFID systems can be higher than in UHF RFID systems when using advanced modulation methods [22].

As for implantation of an RFID device, passive systems are preferred in the long run because of the elimination of expensive battery replacement surgeries. Throughout the literature, implantable devices in the existing volume conduction experiments are LF systems [20, 23]; however, as the result of the progress of technology, the major passive RFID systems seen in the market nowadays are HF and UHF systems with major suppliers as Magellan, SAMSys and Tagsys. Therefore in this work, the more modern RFID systems from Magellan and SAMSys will be used as the RFID reader and device in the experiments and prototype systems.

### **2.1.1 HF RFID system**

HF RFID systems, due to their fast data rate, can be read and written to hundreds of tags within only one second. Currently they are widely used in the applications of logistic warehouse

management, automotive manufacturing, tracking, retail, hospital, baggage check, library management, parcel tracking, security and smart cards. The corresponding ISO standard for HF RFID systems is ISO 18000-3, which details the design and the operation of the HF tag and its communication protocol. Magellan Technology, a manufacturer that utilizes the phase jitter modulation to obtain a higher data rate, is one of the leading suppliers of the HF RFID systems. It has the Mars series readers with stack and item tags and chips along with management software in its product line (figure 2).

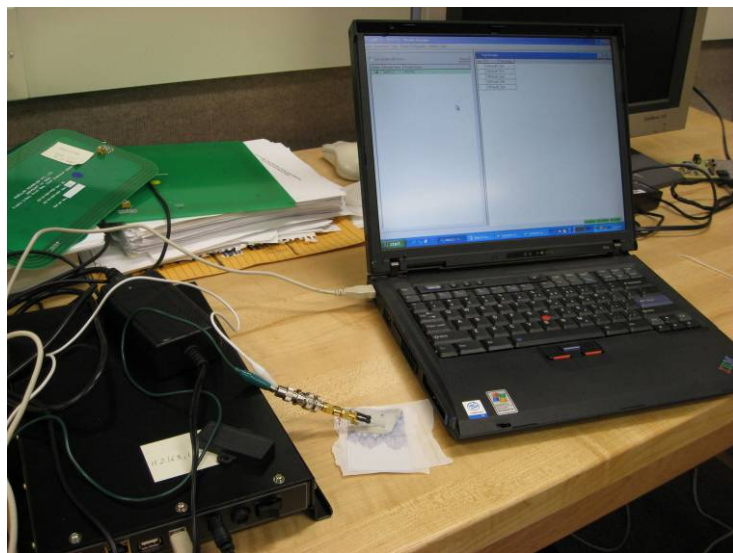


**Figure 2.** The Magellan HF RFID system

### **2.1.2 UHF RFID system**

UHF RFID systems are more up-to-date and more popular in today's research and market, not only because they have higher data transfer rate and faster read/write speeds, but also they have much longer operation ranges than HF RFID systems. Accordingly, the major applications of UHF RFID systems focus on retail, toll roads, and logistics - inside a factory and through the supply chain and long range applications and item tracking as well. However, a hospital room is

more conducive to HF than UHF because UHF signals from a neighboring room could result in unwanted reads [24]. One of the most recent standards for the second generation for UHF RFID systems is ISO 18000-6c, which provides details in the modulation, commands and timing operations for design of UHF readers and tags [25]. Figure 3 shows the UHF RFID systems in the RFID Center of Excellence at University of Pittsburgh.



**Figure 3.** The SAMSys UHF RFID system

## **2.2 PROBLEMS WITH EXISTING SYSTEMS**

### **2.2.1 Metallic interference**

Because orthopedic implants are mainly made from metal, such as stainless steel and titanium alloy, for durability and strength considerations, one major problem of embedding RFID devices on the implanted joints is metallic interference. It is well known that the interference with metallic objects may cause a huge reduction in the level of power captured by an RFID tag [26,

27, 28], which in turn can break the communication link between the reader and the tag and even cause the failure in tag operation. This is because the induced eddy currents by the electromagnetic field radiated from the reader also generates a field that has a counter effect to the original one. Because a metallic object is a good conductor in which the eddy currents are significantly large, the counter field generated therefore can be large enough to reduce the field around the orthopedic implant to a level lower than the threshold for tag operation. However, failure in operation of a tag attached to a metallic object is a case by case problem related to the size and shape of both the metallic object and the tag. To study the feasibility of operating a tag embedded on orthopedic implants through traditional wireless methods, experiments have been conducted on reading a commercialized embedded tag attached to an actual knee joint implant made from titanium.

In these experiments, a Magellan Mars-II reader and a Magellan IT tag designed for implantation have been used. Test configurations in localization of the tag and the artificial joint are shown in figure 4. Repeated read operations are performed in the experiments with each test configuration. For this first configuration, the tag is placed immediately under the metallic part of the knee implant (figure 4(a)); while for the second configuration, the tag was moved a little further away from the metallic part (figure 4(b)). Under the first two configurations, no reading of the tag was seen to be recorded. In the third configuration as seen in figure 4 (c) in which the tag was placed far from the joint, the tag was read with very low efficiency meaning that during N times of reading, the tag responded only for a small number of times. In the last test, two parallel antennas have been used as shown in figure 4 (d) for the first two configurations to increase the field transmitted to the tag. However, again no reading of the tag was seen to be recorded. Based on these test configurations and test results, it is clear to conclude that

traditional wireless methods in operating an RFID device embedded on metallic objects is not an effective method in that a large portion of power from the electromagnetic field is absorbed by the orthopedic implant; an alternative method must be applied.

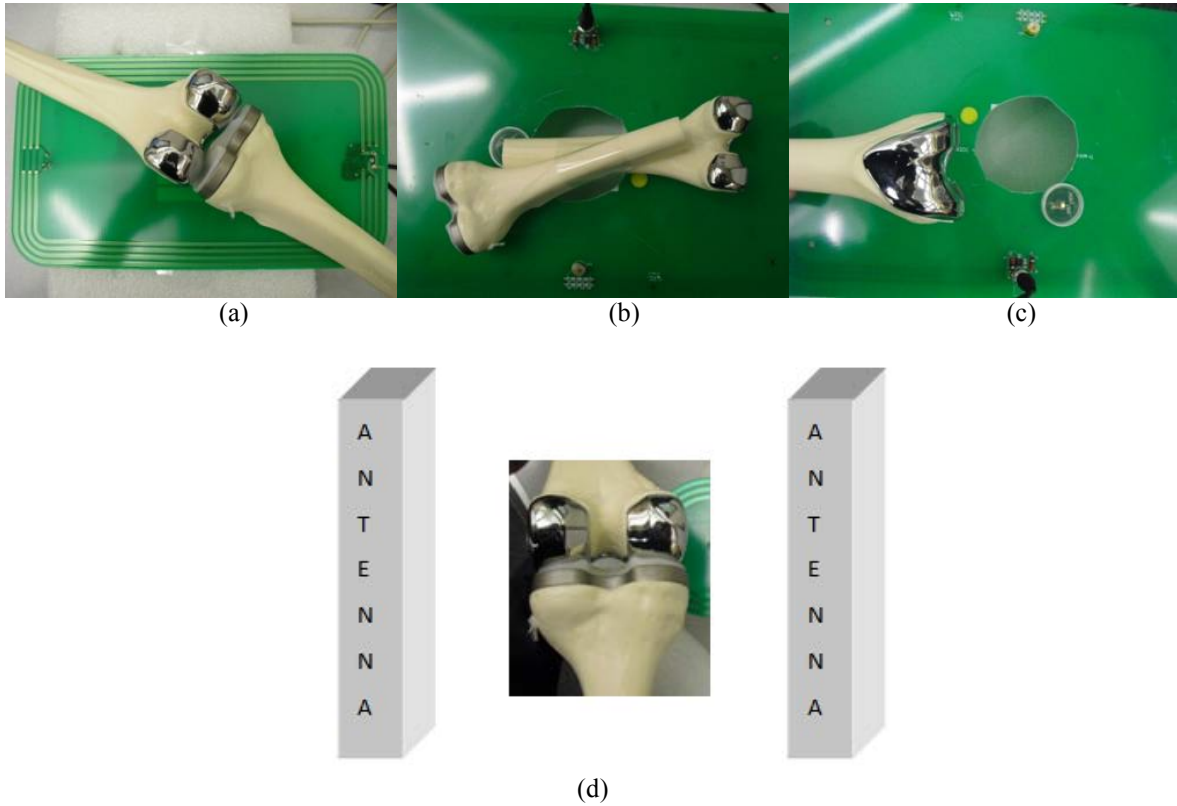


**Figure 4.** Test configurations for RFID metallic interference using wireless way

The current solutions to avoid tag operation failure in such a metallic interference environment include increasing the size of the tag and using multiple antennas from reader. The first solution increases the area of the tag so that more of the electromagnetic field and thus more power can be captured [29]; the second solution uses multiple readers so as to strengthen the field around the tag [30]. However, neither of the two solutions is practical if applied to an orthopedic implant: first, there is little flexibility in the size of tag for the *in vivo* environment – the size of tag must be small enough so that it can be implanted; second, there will arise potential risk to the human tissue according to the regulation for implantable devices; third, interference will occur

with coexistent medical devices (e.g. pacemaker, if any) when more power is radiated [31]. Therefore, the major task of this dissertation is to address this issue by incorporating an RFID system with volume conduction.

### **2.2.2 Signal attenuation through tissue**

Signal attenuation is an important issue in selecting operating frequency and method of operation. Unlike free space in which signal has little attenuation when going through, tissue is a material that significantly absorbs the RF field traveling through. Large signal attenuation will result in failure operation of the RFID tag because of degradation of the electromagnetic field. Signal attenuation also has a major impact on the operational range of the RFID system with a far less effective transmission distance than in the air.

Signal attenuation through tissue is frequency dependant accordingly to [32, 33]. As frequency increases from HF to UHF, attenuation continues increasing before arriving at a peak value. The peak values may vary at different frequencies through different tissues, however, it is obvious that attenuation at UHF is much larger than that at HF. The comparison between using an HF system and a UHF system is detailed at the last chapter. Discussion on signal attenuation and preliminary experimental results are detailed in section 2.4.

## **2.3 VOLUME CONDUCTION**

Studies have shown that ionic fluids within biological tissues are capable of conducting electrical current which, when intentionally manipulated, can be used to transmit both information and

energy. This method of using the body as a conductor, known as volume conduction, has been developed to transmit information from a sensor implanted within the leg of a cadaver to perform mechanical measurements [34, 35], and send information using a body bus described in a Microsoft patent [36]. Although volume conduction has been used mainly for communication in the past, it has shown that the method can be used to transfer sufficient energy across skin to recharge a battery comparable to that of inductive coupling [37]. In a recent study, volume conduction has been utilized experimentally to recharge the battery of an implantable device to avoid battery replacement surgeries [38, 39]. Furthermore, because of the emerging technology in ASIC design, there have been many ultra low power electronic products including those with medical applications, making it possible to power an implanted device through tissue. Because the volume conduction system uses mainly the electric field in conducting power, it has fewer chances to induce large eddy current in metals, and therefore is more power efficient with less interference in a metallic environment than using wireless method of operation. The utilization of volume conduction based RFID system also eliminates the need of antenna, which in turn makes it more flexible in designing the size and shape of the Ortho-tag.

### **2.3.1 System architecture**

A typical volume conduction system includes a source, a load and two pairs of electrodes one placed on the surface of tissue and the other under the tissue (figure 5). The source is placed in contact with the tissue through the external electrode pair. An electric field is generated when a voltage is imposed across the external electrodes. The conductive tissue consequently becomes the carrier for electricity transmission from the external side to the internal load under the force of the high frequency electric field. Two internal electrodes connecting the implantable device are

implanted to interact with the electric field to capture energy and signal to power the load as well as for communication. The implantable device can be an assisted device such as a deep brain stimulator, a monitoring device such as blood pressure sensor or PH level sensor, or an RFID tag. Using this architecture, the implantable device can backscatter information through the inverse path with the same principle.

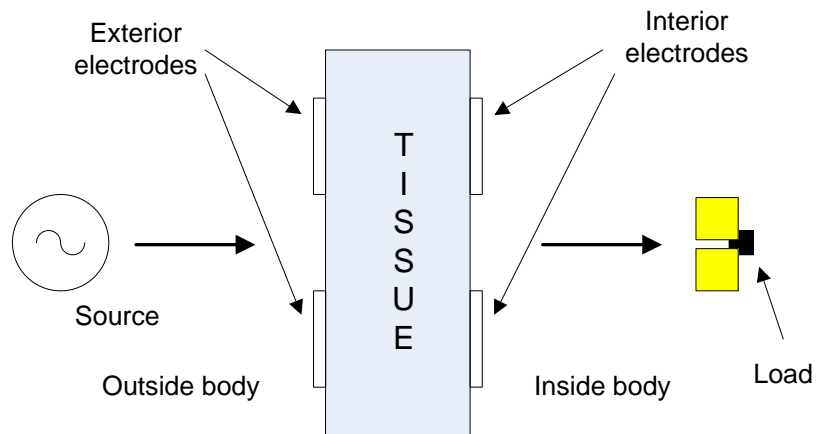


**Figure 5.** A typical volume conduction system

### 2.3.2 Electrodes patterns

The electrode-skin connection is a very important part of any volume conduction system and must be addressed. High impedance connections between the skin and either external or implanted devices can severely degrade signal integrity and dissipate power that could otherwise be delivered to other parts of the system. Quality electrode connections are essential for good performance and long term reliability of the volume conduction system. Given that the system requires charge to actually pass between the external controller, the skin, and the implantable device, a faradaic electrode-skin connection is desired [40].

According to [39] (Hackworth 2010), electrode separation plays a large role in keeping current transmission efficiency high, and a basic geometry of two separate electrodes gives better results than concentric circles or an electrode array. In Hackworth's dissertation, various physical electrodes were originally created with small profiles for testing of the circuit, whose size restrictions on these electrodes were simply too drastic, however, greatly inhibiting system performance (figure 6).

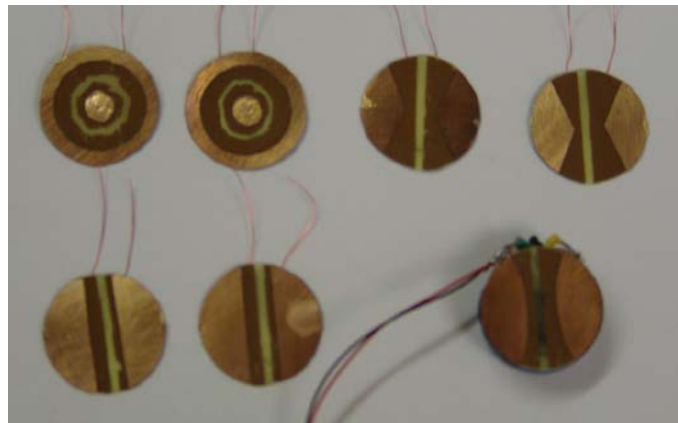


**Figure 6.** Existing patterns of electrodes in [39]

In addition to the electrodes with small profiles, electrodes with round, rectangle and triangle shape were also compared through current efficiency, and the conclusion is that the best efficiency can be obtained through their final configuration of electrodes as shown in figure 7, which combines the advantages of round and rectangular electrodes.

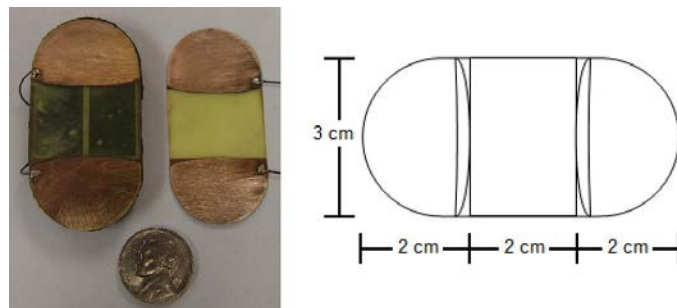


**Figure 7.** The optimized electrode design in [39]

### 2.3.3 Matching networks

In an efficient power transmission system, no matter if it is wireless or wired, matching networks are usually essential parts to optimize the system performance. When the values for matching impedance are known, a matching network between the load/source and the tissue can be designed. A matching network is a circuit consisting of inductive and capacitive components with selected values to transfer the load impedance to the designed one. One well-known matching network is a transformer that increases or decreases the impedance by a ratio equal to the square of the transformer's ratio [41]. Transformer or transformer-equivalent structures that match an RFID chip to the antenna have already been developed as inductively coupling feed which can be single and double T-matching [42, 43, 44]. Similar technologies have also been developed for matching at the UHF [45].

Another simple matching network is the L-section network [46, 47], with components only including inductors and capacitors, which has four configurations in shunt or series connections. This matching network is widely used for RFID systems, with antennas serving as the inductor. Even though the L matching network has drawbacks such as no controllability in the quality factor and bandwidth, it has a simple structure and therefore can be made compact in the layout. Due to the limitation of power being able to be delivered to the RFID device, as well as the limitation of space on an orthopedic implant, the L-section matching network is beneficial and can be incorporated with the RFID device in the HF Ortho-tag RFID system when packaged components are used .

The two above matching networks are passive matching networks; however, more complex matching networks than those can actively adjust the output impedance of the network according to the input impedance. The automatic matching network is one of the active matching

networks which has a matching microcontroller and a series of electronic switches. By controlling the status of the switches, the matching network controls its output impedances at real time to compensate the loss of power in the system [48]. However, the strong matching capability also requires much more power consumption than passive matching networks which is usually not affordable to the Ortho-tag RFID systems.

## **2.4 VOLUME CONDUCTION BASED RFID SYSTEM**

Even though there are systems using volume conduction experimentally realized for transmitting both signal and energy, the implantable devices reported in the existing volume conduction systems are those run with a battery and operate at low frequencies below 1 MHz. However, an effective power delivery scheme in volume conduction systems for passive RF devices is crucial in that passive devices are more sensitive to power and totally rely on the power transmitted through tissue. This is especially true for RFID devices as a good impedance matching circuit can tremendously increase the amount of power captured by the RFID device and thus increase the range of operation. Unfortunately, there have been no studies published for matching any passive RFID devices or even battery-powered implantable RF devices to human tissue. The lack of the matching scheme makes it difficult to determine the optimal value that the load impedance should be matched to which consequently makes the whole system less efficient in power transmission and the operational range.

Furthermore, at operating frequencies of HF and UHF, the two frequencies that are commonly used in the present RFID systems, volume conduction systems have not been designed and studied. Even though the current systems operate at low frequencies, they provide a good

reference for studying the volume conduction based RFID system at higher frequencies. There can still be many differences and even many modifications needed as the field distribution changes and signal attenuation increases when frequency rises. The difference in turn can lead to the redesign and optimization of the electrodes. One illustration of such difference can be achieved from the analyzing the field distribution in which the skin effect at higher frequencies causes more current to be concentrated along the border of the electrodes.

## **2.5 PRILIMINARY STUDIES**

Because there is no previous work for volume conduction based RFID systems which the Ortho-tag RFID system relies on, preliminary studies were conducted as an exploration of viability. As previously discussed, interference with metallic objects and signal attenuation through tissue are major problems for an RFID system to be implanted with orthopedic implants, it is crucial to know how much signal is attenuated in such an environment. In this section, experiments on signal attenuation through tissue with and without metallic interference have been conducted, and read/write operation of an implanted tag using volume conduction was performed as the demonstration of the feasibility of the proposed Ortho-tag RFID system. When measuring the signal attenuation, different sizes of electrodes were carefully selected for comparison. A stainless steel plated (figure 8) is used to generate interference with the electric field between the exterior electrodes and the interior electrodes.

Rather than using tissue, which is costly, uneven in thickness and hard to obtain, 0.17% saline solution, the standard saline solution specified for electromagnetic compatibility tests between RFID systems and medical devices, is used for measuring signal attenuation [49]. The

experimental platform for signal attenuation measurement includes a container filled with saline, round electrodes with variable sizes, a function generator and an oscilloscope. The feasibility tests for read/write operations of the Ortho-tag RFID system were implemented at both HF and UHF frequencies through fresh pig skins.

### **2.5.1 The saline container**

The saline container (figure 8) is built for studying signal attenuation through biological tissue where volume conduction is implemented. The container, made from 9 mm thick acrylic boards, is shown in figure 8. The dimensions of the container are 300 mm x 300 mm x 280 mm in order to hold enough saline to cover a sufficiently large transmission range. The exterior electrodes are attached on the inner side of one of the walls making placing them in direct contact with the surface of the saline. The interior electrodes are attached to a movable panel that can adjust its distance to the exterior electrodes. Stainless screws are used for fastening the electrodes to the container and the panel and also serving as external terminals. By moving the panel toward or away from the exterior electrodes, the distance for signal going through can be adjusted. The maximum distance allowable for the adjustment is 300mm, however, due to weakened signal at a far distance does not guarantee the success of tag operation, signal attenuation was measured up to 50 mm between the exterior electrodes and the interior electrodes.

To study how metallic object affects signal attenuation through volume conduction, a 5 mm thick stainless steel sheet with size of 50 mm by 80 mm is attached between the movable panel and the interior electrodes serving as the metallic orthopedic implant. To insulate the interior electrodes from the metal sheet, another 0.4mm plastic sheet is placed between them to avoid shorting the electrodes by the metal sheet.

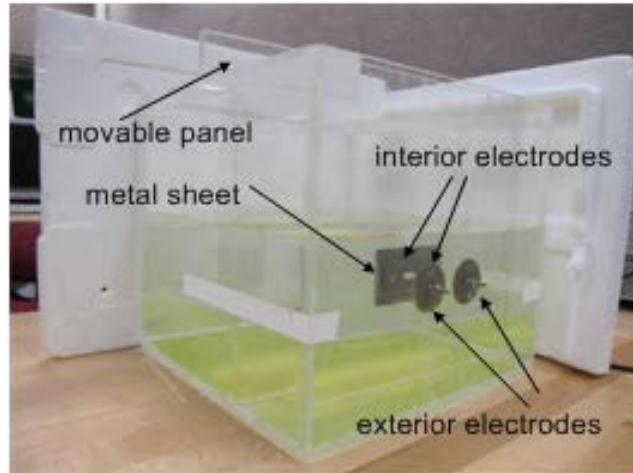


**Figure 8.** The saline container for signal attenuation measurement

### 2.5.2 Electrodes in experiments

Electrode design is one of the most important factors for volume conduction systems. Various electrodes in shape, size and patterns are designed to fulfill different applications [39, 50]. Without losing generality and for the ease of comparison, the electrodes in the signal attenuation experiments are chosen to be the commonly used dipole electrodes with round shape but of different sizes. The electrodes are made of stainless steel to prevent corrosion in saline. The sizes of the electrodes range from 40 mm to 10 mm in diameter, a reasonable for ordinary people. Each electrode is with a centered through hole for screws for holding purpose (figure 9). The thickness of the electrodes is 1mm, making it suitable for implantation.

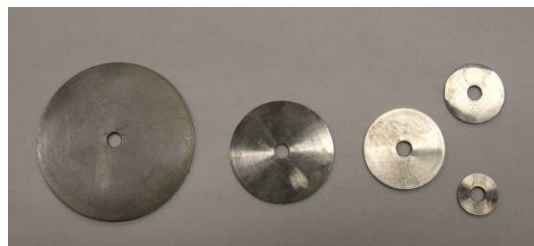


**Figure 9.** Round electrodes with variable sizes

### 2.5.3 Signal attenuation

Because of the lack of prior results in signal attenuation through tissue using different electrode configurations at a specific frequency, it is crucial to measure the attenuation when using different sizes of electrodes with different distances between electrodes. Such experiments are conducted using the saline container previously described. In these measurements, the two exterior electrodes are selected to be 40 mm in diameter with 50 mm between each center. The exterior electrodes are placed and fixed as a pair at the center of the wall at one side of the saline box, which makes them equal in distance to the side walls of the box and to the bottom. The interior electrodes are aligned with the exterior electrodes in such a manner that their flat surfaces are in parallel and they have the same height to the bottom of the saline box from their centers. Because the *in vivo* space is limited for the Ortho-tag, the sizes of interior electrodes are then selected to be in the range between 25 mm to 10 mm in diameter with a 5 mm decrement between sizes. The distance between the two interior electrode centers has a maximum dimension of 50 mm.

In the measurements, the source is a function generator that outputs an 18dBm sine wave at 13.56MHz, the operating frequency of an HF RFID system. The RMS voltage across the exterior electrodes and the interior electrodes are measured using a digital phosphor oscilloscope. The results with the metal plate as an interference source and without the metal plate are shown in figure 10 where the signal attenuation is defined as in equation (1). The letters “L” and “D” in the following figures represent the distance between the center of the interior electrodes and the diameter of the interior electrodes respectively. The saline depth is the distance of saline that the RF signal goes through in the experiments.

$$A = 20 \log_{10} \left( \frac{V_{input}}{V_{output}} \right) \quad (1)$$

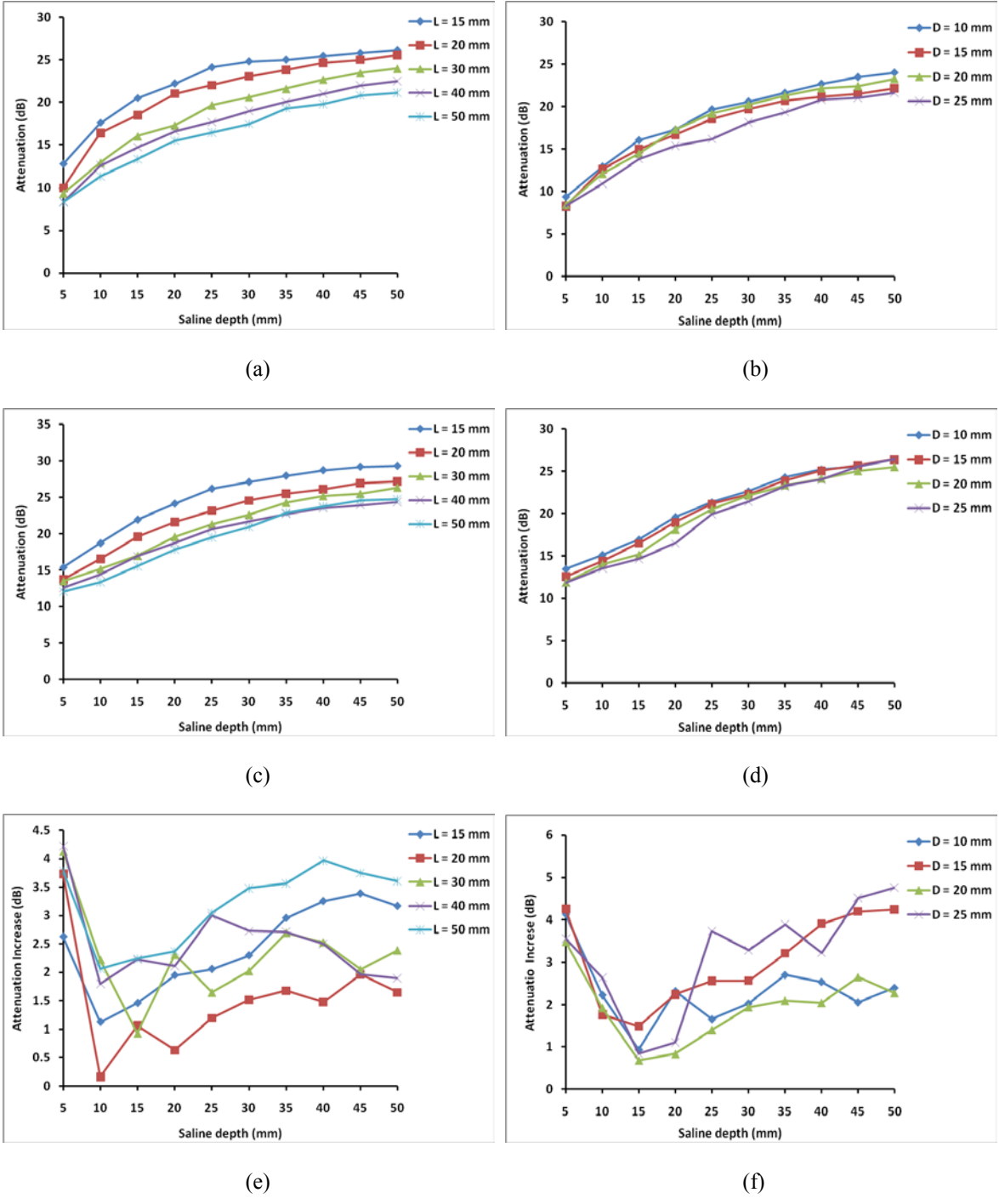


**Figure 10.** (a) signal attenuation without the metal sheet:  $D$  is fixed to be 10 mm ; (b) signal attenuation without the metal sheet:  $L$  is fixed to be 30 mm ; (c) signal attenuation with the metal sheet:  $D$  is fixed to be 10 mm ; (d) signal attenuation with the metal sheet:  $L$  is fixed to be 30 mm; (e) increase in signal attenuation from (a) and (c); (f) increase in signal attenuation from (b) and (d).

The average signal attenuation increase when applying the metal plate to interference with the RF field through volume conduction is 2.38 dB, meaning an equivalent average loss of 24% in voltage efficiency. Even though efficiency is reduced by almost one fourth, resulting in a shorter operation range, compared with the conventional wireless method through which no successful tag operation was recorded, one can make the conclusion that the attenuation increase caused by the metal is relatively small and will not cause a failure in the operation of an RFID tag. Therefore, one can believe that through volume conduction, a metallic object does not cause a severe interference, and operating the Ortho-tag through volume conduction is a feasible method to address the interference issue.

#### **2.5.4 Experimental demonstration**

The prototype of the Ortho-tag is built on a printed circuit board (PCB) to accommodate both the RFID chip and the matching circuit. Following the principle that the tag should be as small as possible under the condition that a reasonable range of operation is guaranteed, the size of the electrodes is chosen to be 10 mm in diameter with 20 mm between the centers of the electrodes. The prototype PCB is then attached to the upper bone of an artificial knee implant (figure 11). An inductor of 10  $\mu$ H is added in parallel with the RFID chip for matching.

The experimental setup includes a Magellan MARS-2 reader, the saline container, a touch probe, the Ortho-tag and the reader console. To simulate the *in vivo* environment, both saline and pig skin were used: figure 12(a) shows the operation of the Ortho-tag through saline and figure 12(b) shows the operation of the Ortho-tag through pig skin. The chip on the tag is designed to allow the usage of an 8 Kb memory with a data rate up to 96Kb/s. This is sufficiently large for storing the information pertaining to the joint and relevant medical information for the patient. In

the experiment, the power of the RFID reader is set to be the maximum, i.e., the same level as the interference test previously introduced when using a wireless antenna.

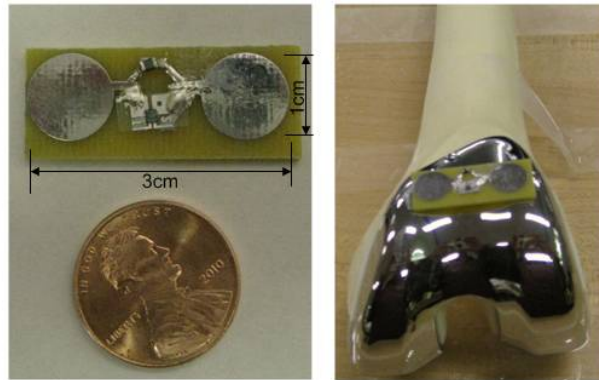


**Figure 11.** The original version of implanted Ortho-tag

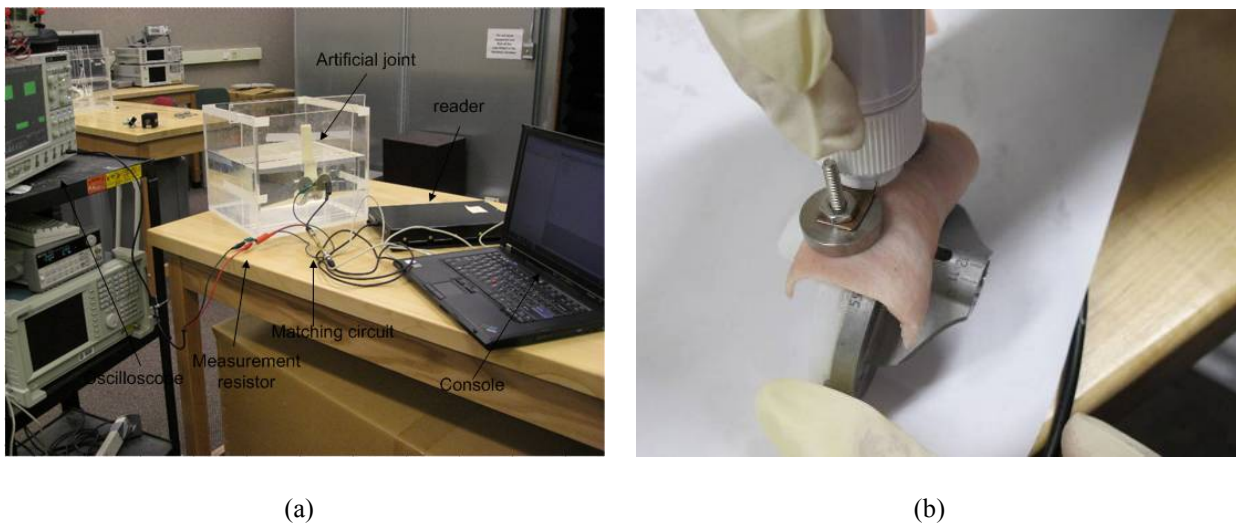


**Figure 12.** (a) Reading the Ortho-tag through saline; (b) reading the Ortho-tag through pig skin

A successful reading distance of 10 mm has been observed during the experiment through saline. This distance is enough for ordinary people who requires knee replacement surgeries. The average current in the saline during the read operation is approximately 76mA, below the safety level specified by [51]. This also allows for increased performance within the limits of safety. At this level of current and taking into account that the reading time for the RFID device is normally less than 1 second, the system proposed will not cause tissue burn and is safe with regard to the human body.

With the average thickness of pig skin being approximately 4 mm, the read operation is performed through multiple layers of pig skin using a dedicated touch probe. The distance readable using the tag is measured in terms of layers of pig skin, with the maximum number being equal to 4, which gives an approximate distance of 16 mm. The experimental results show that no severe attenuation increase is encountered when the RFID tag is placed in the metallic environment of an orthopedic implant using volume conduction. The success in reading the prototype embedded RFID device proves the feasibility of operating an implanted RFID in the metallic environment of an orthopedic implant. Volume conduction is the best approach for an RFID system to reduce metallic interference when considering the human body.

### **3.0 SYSTEM DESIGN**

This chapter describes the proposed Ortho-tag RFID system, spanning from the introduction of the system design as a whole to the discussions on the essential system components including the touch probe, the tag and the reader. Each component acts as an individual system although being linked to each other by matching networks for performance optimization. Configurations of the reader and the tag are discussed along with concerns on the power modes and commands. Software that manages the operation of the system is also discussed with reader-PC interface design for recording the patient registry of an orthopedic surgery.

#### **3.1 PROPOSED ORTHO-TAG RFID SYSTEM**

The proposed Ortho-tag RFID system in this work relies on the same principle as in section 2.3 with an RFID reader being the source and the RFID chip being the load. The major parts are two pairs of electrodes with one pair placed on the surface of tissue and the other pair under the tissue. However, in the Ortho-tag RFID system, the two basic devices are a handheld touch probe and an Ortho-tag with the two pairs of electrodes being a part of each of them. The touch probe, comprising the two exterior electrodes, is connected to the reader through a coaxial cable. It is designed to be held by a surgeon or other medical professional and attached onto the surface of skin when a read or write operation is being performed. The Ortho-tag, consisting of the two

interior electrodes, is placed inside body under the skin on the orthopedic implant for power and command reception through the skin. The RFID reader is at the external side with its output power being applied to the skin through the touch probe. The RFID chip is on the Ortho-tag as a part of it whose power is obtained from the two interior electrodes.

Two matching networks are incorporated with the Ortho-tag RFID system so as to make the system more power efficient. One matching network is placed between the exterior electrodes and the reader as part of the touch probe to match the impedance of the external tissue from the touch probe to the impedance of the reader to eliminate signal reflection. The other matching network, as part of the Ortho-tag, is placed between the interior electrodes and the RFID chip to match the impedance of the chip to the rest system seen from the internal side in order to maximize power transmission efficiency. The diagram of the Ortho-tag RFID system is shown in figure 13.

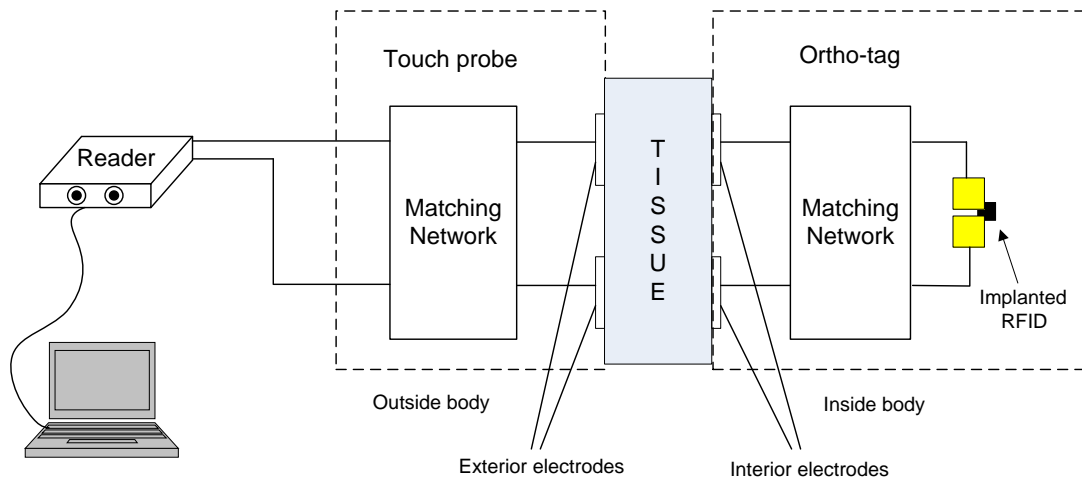


**Figure 13.** The proposed Ortho-tag RFID system.

A computer that connects to the RFID reader is also a part of the system. A Console application on PC is required to provide an operational interface between the Ortho-tag RFID system and the surgeons through which surgeons can use the system for a set of operations such as memory operations and input power level adjustment. The console manages the

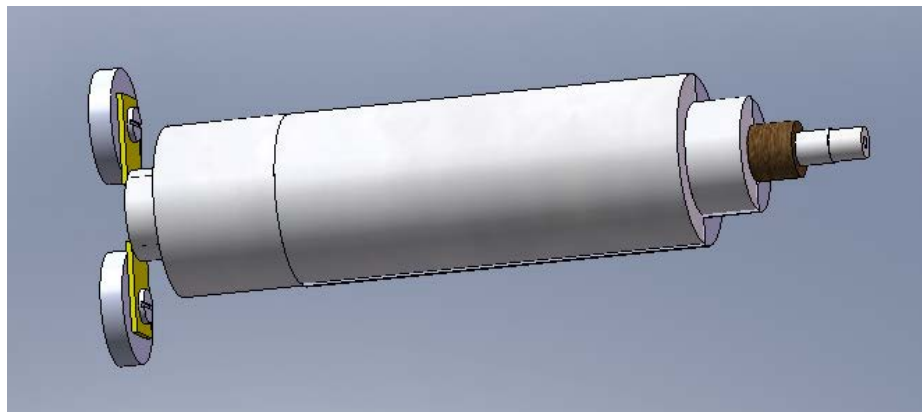
communication between the Ortho-tag and the reader using a user interface. The interface with a patient registry to the Ortho-tag and the export of the registry information to the reader are also necessary fundamental functions of the console. The console application also has an interface to a database which is for recording the history of the operation and the replacement. The detailed introduction of the console application software is discussed in section 3.5 including its architecture and flow chart with corresponding test work.

## **3.2 TOUCH PROBE**

### **3.2.1 Structure of the touch probe**

The touch probe comprises two electrodes, a matching network, a handheld case and a probe-to-reader connector. The electrodes are the part that is placed in contact with the tissue to diffuse power from the RFID reader to a certain area of tissue to form an electric field. The matching network is designed to match the electrodes to the RFID reader so that maximum power can be delivered to tissue to maximize the electric field strength. The matching network directly connects to the electrodes at one end and connects to the cable of the RFID reader at the other side through a specified connector. Two designs of the touch probe are proposed and implemented as in figures 14 and 15, for use with different applications from HF Ortho-tag RFID system to UHF system with considerations of system efficiency and flexibility in incorporation of the matching network. One major feature to increase system performance and design flexibility of each proposed touch probe is that the electrodes are replaceable and the distance between electrodes is adjustable. This feature assists the matching of the touch probe in the following two aspects. First, the

changeability of electrodes makes it more convenient to use a proper pair of electrodes for a patient, in size and shape, which can increase the electrode-to-tissue efficiency. Second, in the case that components in the matching circuit, such as capacitors and inductors which are not always available for specific values, adjusting the distance between electrodes can change the impedance of tissue at the external side in a small degree, and therefore is able to assist matching the tissue and electrodes to the optimal value.



(a)

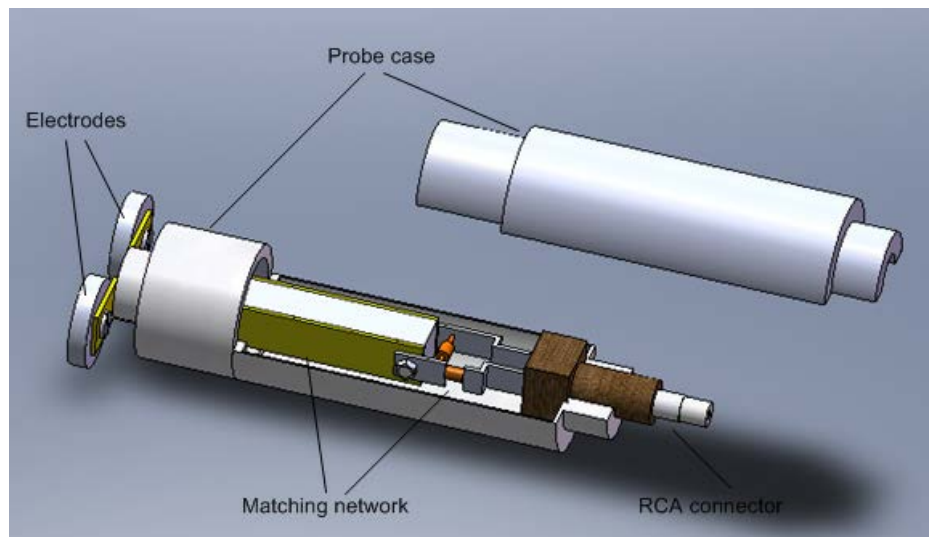
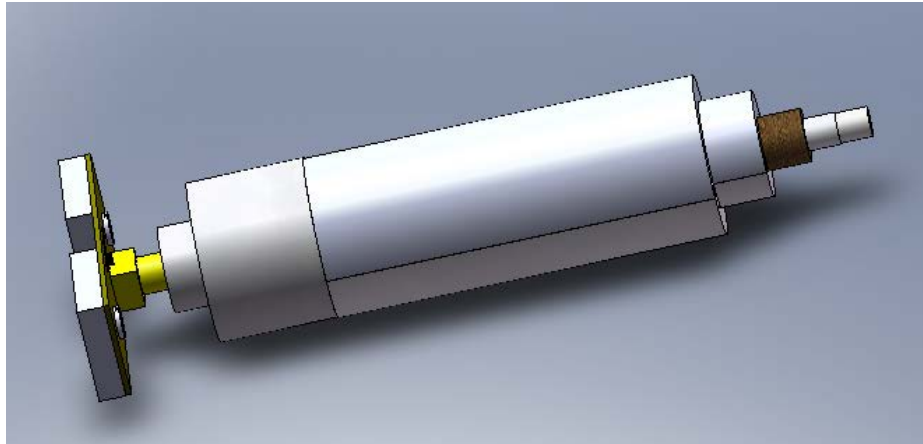
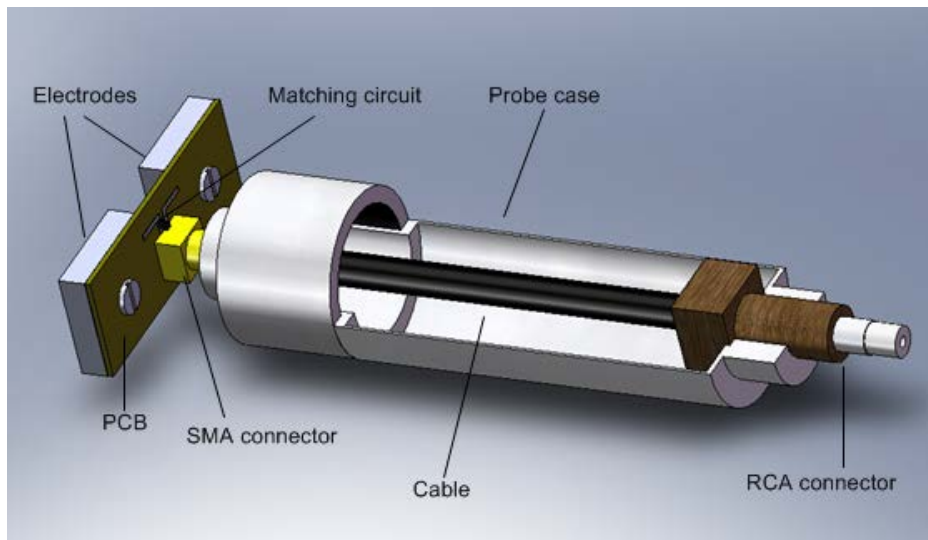


**Figure 14.** (a) The HF touch probe; (b) inner display of the HF touch probe



(a)



(b)

**Figure 15.** (a) The UHF touch probe; (b) inner display of the UHF touch probe

The HF touch probe has two round electrodes, made from stainless steel and a cylindrical case, and the other end is an RCA connector for the cable with Magellan Mars-2 reader. Other shapes of electrodes such as rectangle or triangle can be used whichever fits the patient. The inside of the touch probe is the matching network and a pair of L-shaped copper bar (the yellow part). The electrodes are attached to the short end of the copper bar through two screws while at the long end of the metal bar the RCA connector is connected by using screws or a solder joint.

The touch probe for the UHF system is different from that for HF system in that a printed circuit board (PCB) is used for the matching network. Rectangular stainless steel electrodes, also replaceable, are used as the primary electrodes because of their larger area within the constraint. The electrodes are then connected to the PCB through screws and are therefore connected to the matching circuit. The other side of the touch probe is an SMA connector, which connects to the matching network on PCB through a coaxial cable to reduce signal loss when transmitting from the read to the PCB.

### 3.2.2 Matching network for the touch probe

The fundamental construction of the matching networks for both HF and UHF touch probes satisfies the rule that an LC circuit be used to match impedance. In this work, for the possibility to make the matching networks in a small compact design to fit the electrodes, an L matching network is used. Because the impedance of tissue is usually less than that of the RFID reader, i.e. 50 ohm, a matching network with series inductor and parallel capacitor is utilized as in figure 16.

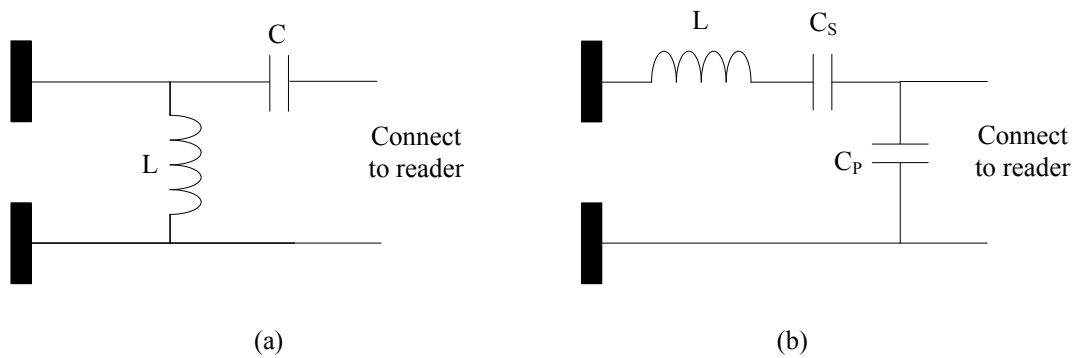


**Figure 16.** (a) Equivalent circuit of the matching network of the HF touch probe; (b) equivalent circuit of the matching network of the UHF touch probe

For the HF touch probe, the equivalent circuit of the matching network includes one capacitor and one inductor which are adjustable for tuning. For UHF touch probe, the equivalent circuit of the matching network includes one inductor and two capacitors with one capacitor in series with the inductor and the other in parallel. Because the inductor is created by the PCB wire at UHF, which is usually difficult to control by only adjusting the wire length and width, the series capacitor is used to tune the inductance of the circuit given a fixed parallel capacitor.

### 3.3 ORTHO-TAG

Two Ortho-tags, one for HF system and the other for UHF system are discussed and implemented in this dissertation, with their electrodes and matching network layout as shown in the following figure.

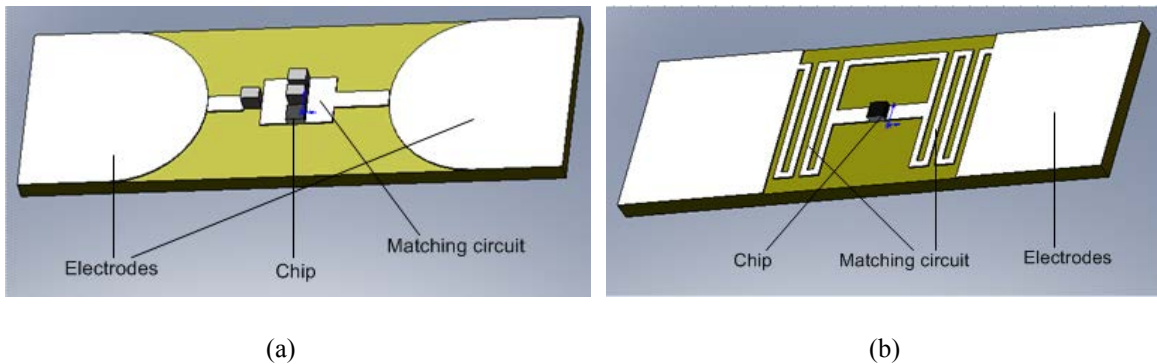


**Figure 17.** (a) HF Ortho-tag; (b) UHF Ortho-tag

#### 3.3.1 Electrode design

As from figure 10, for HF Ortho-tag RFID system, the larger electrodes with larger distances between them tend to have smaller signal attenuation as the thickness of saline increases. As to

the distance between interior electrodes, a longer distance between the centers of interior electrodes indicates a longer path for the electric field from one electrode to the other and, as a result, the integral of the electric field along the path, being equal to the voltage drop between the electrodes is larger. As to the size of electrodes, with the interior electrodes growing larger, consequently more interference with the electric field (i.e. more coupling with the touch probe) can be detected, resulting in a larger current on the interior electrodes. Large current on the interior electrodes means more capability of the electrodes in driving the load which, in turn is equivalent to provide a significant voltage across the load. Therefore, for the HF Ortho-tag, to optimize its electrodes in shape, a combination of round and rectangular shapes are used as in figure 17(a) where a round curve is applied to the inner border between the electrodes to enlarge the effective distance between the electrodes, and a rectangular outer border is used to increase the overall area.

As for the UHF Ortho-tag, due to the fact that a small piece of wire can capture power as an antenna, its power reception comes from both volume conduction and radiation. Therefore in the UHF system, the increase in the effective distance by curving the inner border of the electrodes is not as important for voltage increase. For the primary consideration of power reception for more volume conduction portion, the shape of electrodes is chosen to be rectangular so that it has a larger area in receiving power than the round ones within the same tag area of constraint. The optimization process of the UHF Ortho-tag optimizes the distance between electrodes as part of the matching circuit to maximize the gain of the received voltage as discussed in section 4.3.

### 3.3.2 Matching network for the Ortho-tag

The matching network on the Ortho-tag follows the same principle as on the touch probe, with a different pattern for implementation. For the HF Ortho-tag, as the impedance of the RFID chip is always much greater than the value to which it should be matched, a capacitor in series with the network and inductor in parallel with the RFID chip are utilized to decrease impedance from the chip to the electrodes (figure 18(a)). A tuning capacitor is also added in parallel with the chip for tuning its impedance due to that it is difficult to find an inductor large enough to match for the HF chip with a large capacitive impedance.

For the UHF Ortho-tag, chip impedance becomes much smaller due to the increase in frequency which can be close to the impedance of electrodes. However, technology using the geometry of a meander-line having multiple unequal turns [52] to reduce the size of a UHF antenna has been invented and verified. Therefore, in this work, a matching network using meander-line with 2 turns is applied to match the chip impedance to the electrodes as shown in figure 17(b). The equivalent circuit of the matching network is shown in figure 18(b). The horizontal lines mainly control the radiation resistance, the adjacent vertical lines give storage of electric energy and loss, and the overall conductor length affects the inductance.

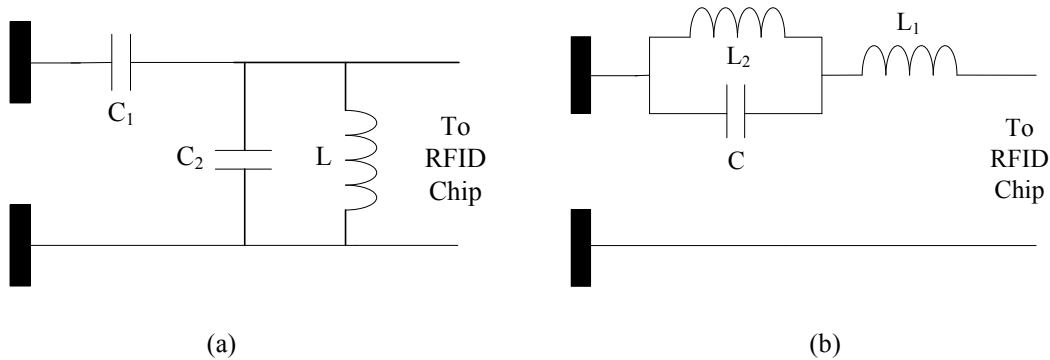


**Figure 18.** (a) Equivalent circuit of the matching network of the HF Ortho-tag; (b) equivalent circuit of the matching network of the UHF Ortho-tag

### 3.3.3 Electrode material

For demonstration purposes, the electrodes in the prototype Ortho-tags are made from copper; however, copper can be irritating to tissue and is not a proper material for clinical applications. This section aims to introduce the electrode materials for the electrodes on the Ortho-tag for implantation purposes with discussions on their appropriateness. Major considerations on selecting the material are the electrode injection limit and the electrode-tissue interface impedance. The foremost conductive materials are metals including two categories namely noble metals and non-noble metals [39]. Metals such as platinum, iridium, and gold are noble metals. Noble metals are highly resistant to environmental corrosion, though corrosive effects such as loss of mass, unwanted film formation, and particulate debris are possible when used with higher current levels [53]. Platinum is the most widely used, though it is usually alloyed with iridium to increase its strength. Iridium is often used by itself in implants, being stronger than platinum, but when used in such a manner, a layer of iridium oxide that results in a low contact resistance on the surface is necessary. Non-noble metals used in implantable devices take advantage of the same type of reversible oxidation process. However, care must be taken not to exceed the charge injection limit because of the resulting irreversible faradaic reaction which dissolves the electrode [54]. Common non-noble metals are stainless steel and nickel-cobalt alloys. These conductors, though mechanically stronger, tend to have smaller charge injection limits than the noble metals and can introduce large impedance. However, a titanium nitride electrode is very stable and capable of high charge injection while maintaining relatively low impedance [55].

### 3.4 RFID READER CONFIGURATION

The main purpose of the reader configuration is to set up the operating manner of the reader and the tag, including power level and behavior when powered on and adjusting power modes. The basic items that can be set through reader configuration include output power level, IP address of reader, connection method to reader, and channel selection. Besides, operations regarding the Ortho-tag such as tag power mode and basic tag operation can also be configured in this process [56]. During the tests throughout this dissertation, all readers are set with the configurations such that the power level of the reader is the maximum and the power mode of tag is normal.

The behavior of the reader after being powered on is an important part in the experiments which can be done through passing a list of commands and functions to the reader server. The behavior includes repeated sending the inquiry command and carry wave to search if a tag is in the range of operation. When a tag is found, the reader sends a read command to the tag and displays its ID in the console window.

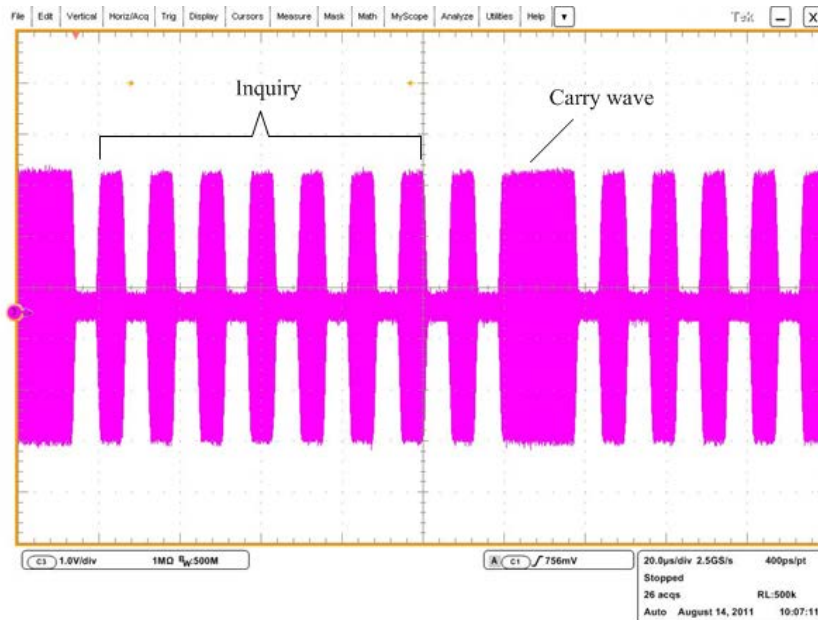


**Figure 19.** Signal being sent after reader is powered on

### 3.5 SOFTWARE DESIGN

The commonly used software is the console application originally distributed with the RFID reader, such as the *ReaderManager* for the Magellan readers and for the Samsys reader. The software with the reader includes every function regarding the operation of the tag involving the linkage between PC and the reader, configurations of the reader, settings for the tag and memory operations, through which one can write up to kilobytes of data into the memory and read those data from the memory. In most of the tests and demos regarding the Ortho-tag RFID System, the originally distributed software with the RFID reader is used; however, the software does not provide a user interface for the patient registry and the database. The redesign to the existing software for the necessary features is not feasible as the reader manufacturers do not provide any authority to modify their software. A software design to incorporate the base tag operations with the patient registry and the database as well as to reduce the operation complexity is necessary for the Ortho-tag RFID system.

The method to link the reader and the PC in a programming language is *socket* [57] as the reader is a common sensed server with an IP address for identification. Each reader has its own commands and functions for its operation, which is usually written in Python or C, according to the reader programming manual [58]. The operations of the reader can then be implemented by sending a series of commands with a certain format through a socket within several steps. The first step is the creation of the socket and verification of its communication to the reader. Upon receiving the information sent from the socket, the identification number and the IP address of the reader are sent back to the same socket from which all the information is to be verified before moving to the next step. The next step is the creation of the commands to be recognized by the reader. These commands are sent to the reader either in binary bits or text, depending on the

software development tool and the reader. After the second step is finished, the reader starts to respond to the commands by doing designated operations, including sending data packages to PC. The third step is then the reception of data, involving data processing and verification, and can be easily done using the modern development tool. The operation cycle for the reader-PC interface using socket is shown in figure 20.

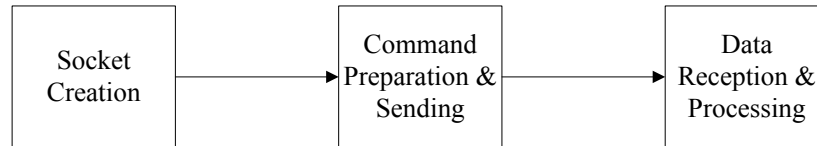


**Figure 20:** A cycle of operating the reader through PC

The flow chart for a read operation is shown in figure 21. The waiting time for response from the reader is 3 seconds, after which the program will enter the error process to fail the link between the PC and the reader. For each read operation, the read command is sent 3 times in case the loss of power during reading caused by touch probe movement. The operation history and the data read from the Ortho-tag are to be displayed as well as to be written into the hospital database.

A program is written in C++ as the interface program proposed for the Ortho-tag RFID system. The test of the proposed software design is shown in figure 22, in which the left part of the figure displays the messages regarding the operations of the Ortho-tag through pig skin in a black window, and the right part is the development environment. During the test, the program first sends packages to request a visit to the reader and receives a response from the reader with information as the IP of the reader, and the version of the reader and its firmware, which are at the beginning of the read window. After the reader is linked by the program, a command package requiring a write operation of 400 bytes to a specified memory location of the Ortho-tag is issued and sent along with a default power level and a normal tag power mode. When the write

operation is finished, another command package requiring a read operation is sent, for obtaining the same length of data from the address to which the previous data are written. The data written and read are listed in the picture with the addresses for each word length of the data. With a size of 400 bytes being big enough for a patient registry in figure 23, and the read/write time for the total 400 bytes being less than 1 second, the proposed software design in the operation of the Ortho-tag is a feasible design to fulfill the need of the Ortho-tag RFID system for patients and hospitals.

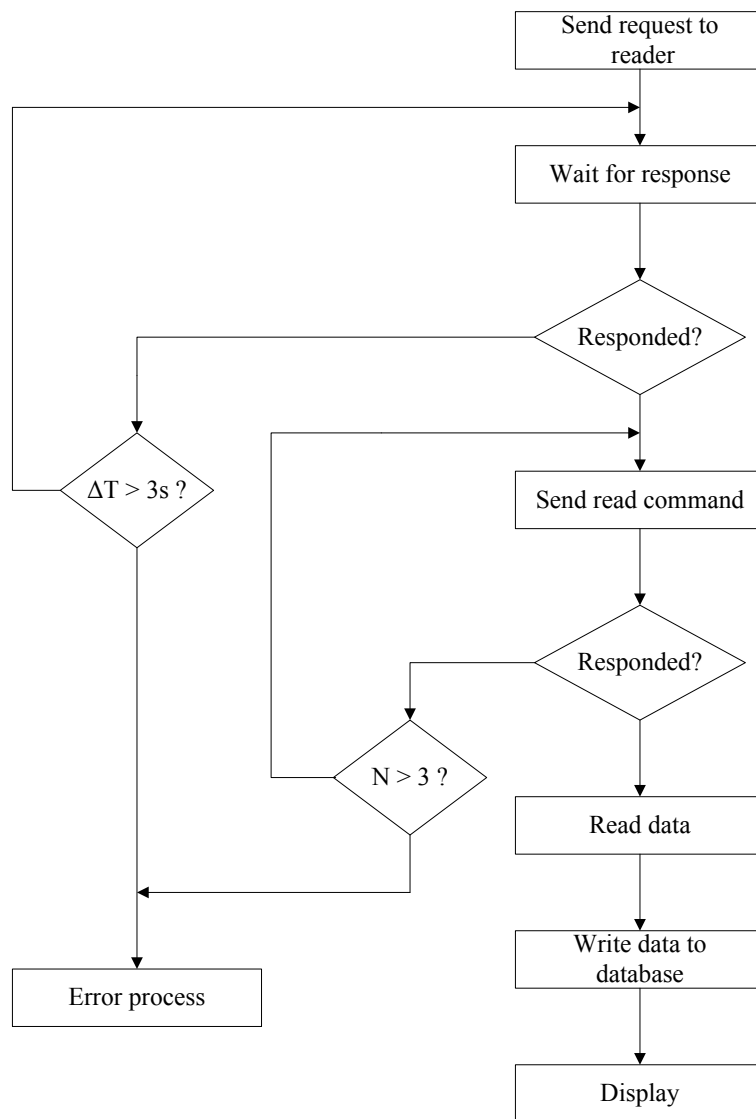


**Figure 21.** Flow chart for the read operation

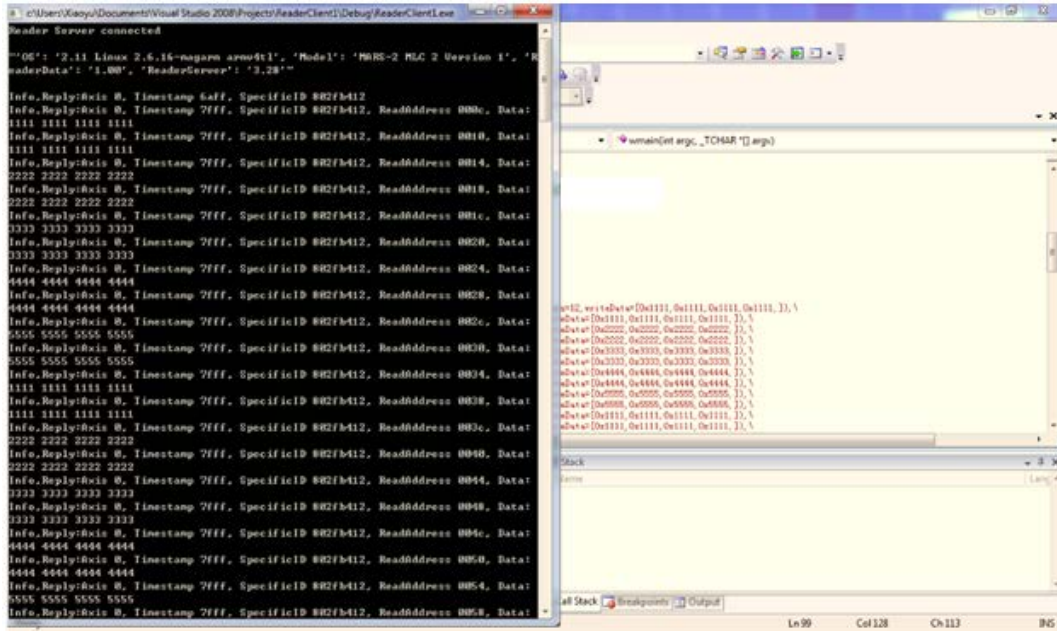


Figure 22. Test of the software design

		<b>LB Medical Ortho-tag Joint Registry</b> <a href="http://www.OrthoTag.com">www.OrthoTag.com</a>	
<b>TKA# Primary TKA</b> Total Knee Replacement			
<small>Important: Please check relevant boxes. All component stickers should be affixed to this form. Please ensure that all sheets are attached together.</small>			
		Ortho-tag Reference Number: _____	
<small>All fields are mandatory unless otherwise indicated</small>			
<b>PATIENT DETAILS</b>			
Patient Consent Obtained	Yes <input type="checkbox"/>	No <input type="checkbox"/>	Not Recorded <input type="checkbox"/>
Patient Hospital ID	_____		
Body Mass Index (Enter value and BMI or check Not Available box)	Height _____	BMI _____	Not Available <input type="checkbox"/>
<b>PATIENT IDENTIFIERS</b>			
First Name	_____		
Last Name	_____		
Gender	Male <input type="checkbox"/>	Female <input type="checkbox"/>	Not Known <input type="checkbox"/>
Date of Birth	Age _____	DDMMYYYY	
Patient Telephone Number	Patient Address _____		
Insurance Number	_____		
<b>OPERATION DETAILS</b>			
Hospital	Hospital Address _____		
Operation Date	DDMMYYYY		
Anaesthetic Type	General <input type="checkbox"/>	Regional - Spinal <input type="checkbox"/>	Regional - Nerve Block <input type="checkbox"/>
Patient ASA Grade	1 <input type="checkbox"/>	2 <input type="checkbox"/>	3 <input type="checkbox"/>
Anaesthesiologist	_____		
<b>SURGEON DETAILS</b>			
Operating Surgeon	Surgeon's Office Address _____		Telephone Number _____

		<b>LB Medical Ortho-tag Joint Registry</b> <a href="http://www.OrthoTag.com">www.OrthoTag.com</a>	
<b>THA# Primary THA</b> Total Hip Replacement			
<small>Important: Please check relevant boxes. All component stickers should be affixed to this form. Please ensure that all sheets are attached together.</small>			
		Ortho-tag Reference Number: _____	
<small>All fields are mandatory unless otherwise indicated</small>			
<b>PATIENT DETAILS</b>			
Patient Consent Obtained	Yes <input type="checkbox"/>	No <input type="checkbox"/>	Not Recorded <input type="checkbox"/>
Patient Hospital ID	_____		
Body Mass Index (Enter value and BMI or check Not Available box)	Height _____	BMI _____	Not Available <input type="checkbox"/>
<b>PATIENT IDENTIFIERS</b>			
First Name	_____		
Last Name	_____		
Gender	Male <input type="checkbox"/>	Female <input type="checkbox"/>	Not Known <input type="checkbox"/>
Date of Birth	Age _____	DDMMYYYY	
Patient Telephone Number	Patient Address _____		
Insurance Number	_____		
<b>OPERATION DETAILS</b>			
Hospital	Hospital Address _____		
Operation Date	DDMMYYYY		
Anaesthetic Type	General <input type="checkbox"/>	Regional - Spinal <input type="checkbox"/>	Regional - Nerve Block <input type="checkbox"/>
Patient ASA Grade	1 <input type="checkbox"/>	2 <input type="checkbox"/>	3 <input type="checkbox"/>
Anaesthesiologist	_____		
<b>SURGEON DETAILS</b>			
Operating Surgeon	Surgeon's Office Address _____		Telephone Number _____
Assistant	_____		

Figure 23. The patient registry

## **4.0 SYSTEM OPTIMIZATION**

This chapter discusses the optimization method of the Ortho-tag RFID system to address the issues on matching the system with orthopedic implants. This chapter includes five sections with a detailed introduction and discussion on the optimization procedures. The first section introduces the simulation tool that is being used for analyzing the performance of the Ortho-tag RFID system with discussions on its features and applications. The second section introduces the Z matrix that describes the transmission relationship between external side and internal side. The third section and the fourth section are the optimization procedures for both HF system and UHF system including electrode optimization, load impedance optimization and the matching network. Two different matching technologies and matching networks are utilized for the HF system and UHF system independently based on the given limitation of the tag size. The last section summarizes the proposed design procedure for the system optimization.

### **4.1 DESIGN TOOL**

The tool used for optimizing the Ortho-tag RFID system is high frequency structure simulator (HFSS), an industry-standard simulation tool developed by ANSYS Inc. for 3D full-wave electromagnetic field simulation and essentially for high-frequency and high-speed component design. Ansoft HFSS can be used to calculate parameters such as S-parameters, resonant

frequency, and fields. It integrates simulation, visualization, solid modeling, and automation in an easy-to-use environment where solutions to 3D EM problems are quickly and accurately obtained. HFSS offers “multiple state-of-the-art solver technologies each based on the proven finite element method, with adaptive meshing and brilliant graphics” [59]. Users select the appropriate solver for the type of simulation they are performing including eigenmode solver, driven mode solver and driven terminal solver. Each HFSS solver is based on a powerful, automated solution process where users are only required to specify geometry, material properties and the desired output of a 3D structure. An appropriate, efficient and accurate mesh for solving a given structure is automatically created with certain manual mesh configurations open to users to increase the density of mesh for detailed field analysis on specific areas.

To analyze the EM field and port parameters for tissue in this work, the driven mode solver in frequency domain [72] is applied in solving the field distribution around the structure of a knee implant with the Ortho-tag RFID system performing a read operation through the skin (figure 24). Several features of HFSS can be used to simplify the model to reduce the total calculations and to accelerate the speed of simulation. Lumped ports are created as the excitations of the model. Lumped RLC boundaries are used for simulating fixed value RLC components and perfect E boundaries are used to simulate traces. Mesh operations are made as default in simulation, which is automatically assigned by the simulator. Material for tissue uses wet skin, with properties of conductivity, permeability and tangent loss from [60].

HFSS also provides an optimetrics package which can be used in finding a better or more suitable design instance among the possible design variations. Optimetrics includes a parametric and optimization analysis module providing an intuitive interface on top of the advanced macro language built into HFSS that lets the users define model parameters which will vary, setup a

data table to specifically control iterations and/or identify performance specifications to optimize. In this dissertation, the optimetrics package is used for optimizing the geometry of the touch probe and tag and for the matching chart as well.

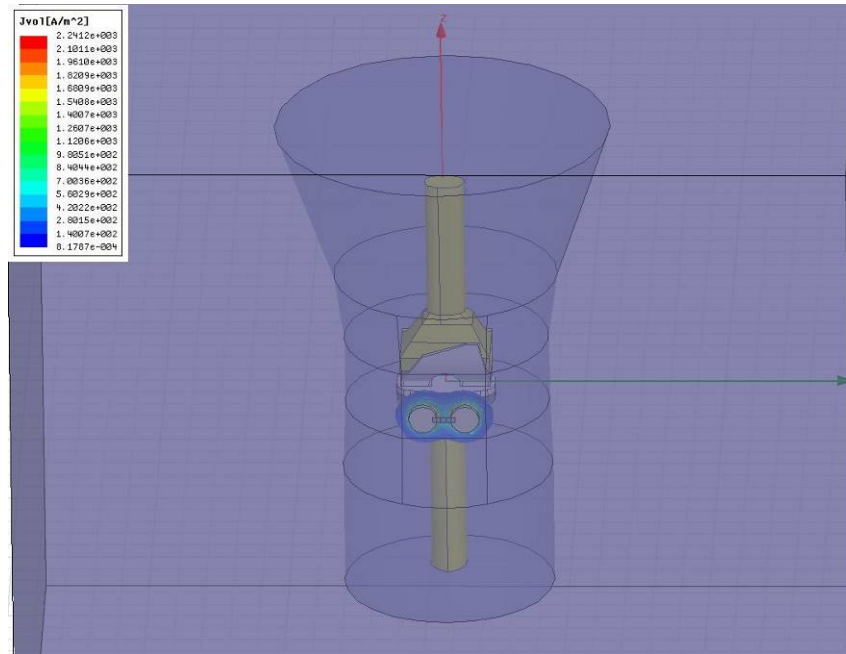


**Figure 24.** The knee implant model in HFSS

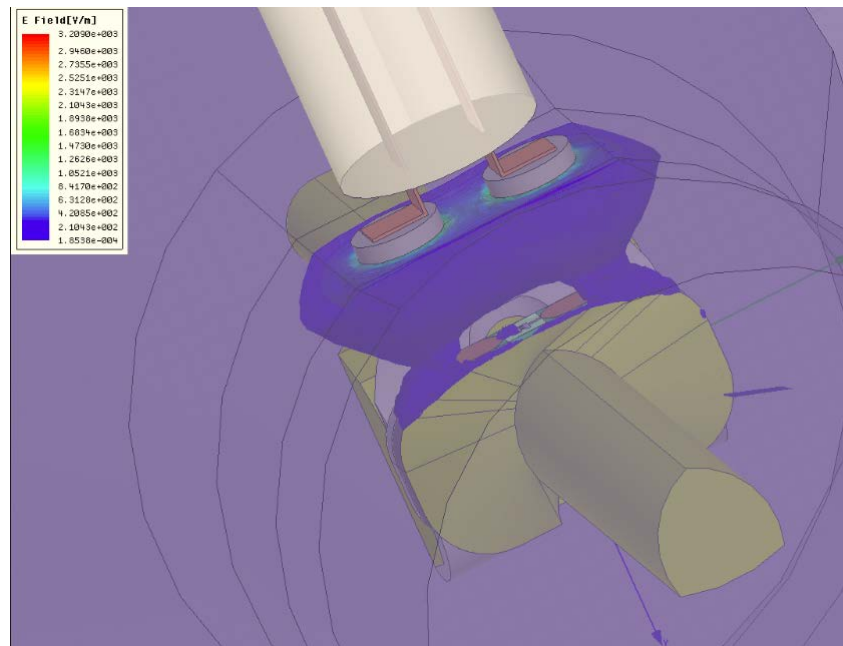


**Figure 25.** The simulated electrical field distribution in tissue

## 4.2 THE TISSUE MODEL

The key to calculating the impedance of tissue is to find an electrical model for the tissue which can specify the transmission features especially the impedances seen from both external and internal sides of tissue. The impedance from the internal electrodes varies with the thickness of tissue as well as the size and shape of the electrodes on the Ortho-tag. The impedance from the external electrodes is not only determined by the tissue and the touch probe, but is also determined by the load on the Ortho-tag because of the coupling between the touch probe and the tag. It is also true with the voltages across the electrodes as they are dependent on impedance. Therefore, the load power can be a function of the load impedance with the two relationships defined: the relationship between the external impedance and the load impedance; and the relationship between the external voltage and the load voltage.

Most literature references consider human tissue as linear circuits [61, 62, 63] with only capacitors and resistors. With the two pairs of electrodes in the Ortho-tag RFID system, a two port network model is then applied in this dissertation. Note that in order to do this, the tissue must be assumed linear so that the above two relationships are linear and are not a function of voltage or current. This assumption is true if the current in the tissue does not exceed its limit and can be controlled by adjusting the input power. Therefore, the above two relationships can be described as two functions only of the load impedance as in equation (2); the impedance seen from either side of electrodes does not change with the voltage or current if the geometry of the Ortho-tag and the touch probe and their location remain fixed.

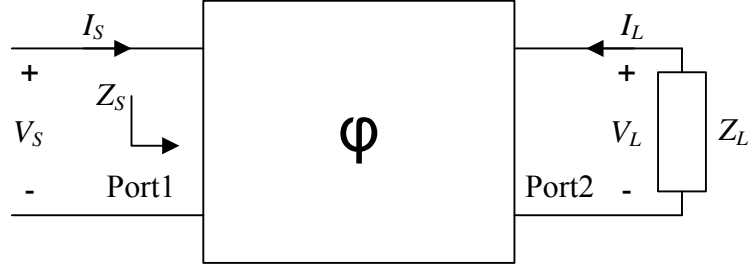


**Figure 26.** Modeling the tissue as a two port network

$$\begin{cases} Z_s = \varphi_1(Z_L) \\ V_L = \varphi_2(Z_L)V_S \end{cases} \quad (2)$$

To derive the two functions in the above equation, finite element analysis (FEM) needs to be performed with the load in two extreme cases: open circuit and short circuit. Voltage and current can then be calculated from integrating the electric field along a certain path linking the voltage and integrating magnetic field around the cross-section of current. The circuit parameters can then be calculated from the voltages and currents at the ports which are determined by the above two functions of load impedance. However, this method is not realistic because the integration must be performed manually which increases the amount of computation and the risk of numerical errors such as in precision and rounding. Alternatively, Z-parameters which are properties commonly used in electrical and electronic circuits to describe the electrical transmission behavior of linear networks can be used to derive the above two functions.

The definition of Z-parameters for the two port network tissue model is equation (3), with direction of voltage and current defined as in figure 26. The left side of the equation is a 2x1 vector representing the voltage across the exterior electrodes and the interior electrodes respectively and the input at the right hand side is a 2x1 current vector representing the current flowing into the exterior electrodes and interior electrodes respectively. The voltage vector and the current vector are linked by Z-parameter matrix, where  $Z_{ii}$  is the impedance from port i with

the current of the other port being equal to zero, and  $Z_{ij}$  is calculated by dividing the voltage at port  $i$  by the current at port  $j$  with the current of port  $i$  being equal to zero. Fortunately, HFSS can generate the  $Z$ -parameter matrix automatically after each simulation if the ports are defined which is more time efficient when using optimetrics and frequency sweep.

$$\begin{bmatrix} V_S \\ V_L \end{bmatrix} = \begin{bmatrix} Z_{11} & Z_{12} \\ Z_{21} & Z_{22} \end{bmatrix} \begin{bmatrix} I_S \\ I_L \end{bmatrix} \quad (3)$$

According to figure 26,  $Z_S$  and  $Z_L$  are defined as:

$$Z_S = \frac{V_S}{I_S}, Z_L = -\frac{V_L}{I_L}. \quad (4)$$

Dividing the first equation of (3) by  $I_S$  and using (4), one obtains

$$Z_S = Z_{11} + Z_{12} \frac{I_L}{I_S}. \quad (5)$$

Dividing the second equation of (3) by  $I_L$  and using (4), one obtains

$$\frac{I_L}{I_S} = -\frac{Z_{21}}{Z_L + Z_{22}}. \quad (6)$$

Combining (5) and (6), the function  $\varphi_1$  in (2) becomes equation (7), where the  $Z$ -parameters are known coefficients from field analysis by HFSS.

$$Z_S = \varphi_1 = Z_{11} - \frac{Z_{12}Z_{21}}{Z_L + Z_{22}}. \quad (7)$$

The function  $\varphi_2$  can be derived by the following two steps, of which the first step is to express  $\varphi_2$  as a function of  $\frac{I_L}{I_S}$  using (3):

$$\varphi_2 = \frac{V_L}{V_S} = \frac{Z_{21} + Z_{22} \frac{I_L}{I_S}}{Z_{11} + Z_{12} \frac{I_L}{I_S}}. \quad (8)$$

The second step is to substitute  $\frac{I_L}{I_S}$  using equation (6):

$$\varphi_2 = \frac{Z_{21}Z_L}{Z_{11}Z_L + Z_{11}Z_{22} - Z_{12}Z_{21}}. \quad (9)$$

### 4.3 HF SYSTEM OPTIMIZATION

This section introduces the optimization methodology for the HF Ortho-tag RFID system including the optimization of the electrodes and matching circuit. Because the matching circuit usually requires inductance at the level of  $\mu\text{H}$ , which is difficult to create only by making traces on tag especially when attached to metal, pre-packaged and shielded IC inductors are used to form inductance in the matching network. Therefore, all the components in the matching circuits are lumped parameters including an inductor and two capacitors. The optimization process will later be the optimization of the LC values.

#### 4.3.1 The electrode optimization

Similar to an RFID system using conventional wireless transmission in which antennas are used for coupling between the reader and the tag, the electrodes on the Ortho-tag play an important role on the coupling between the touch probe and the Ortho-tag and thus affect the transmission efficiency tremendously. As in a typical RFID system where antennas are optimized for high gain, the aim of electrode optimization is also to maximize the coupling and power delivery by optimizing the shape, size and installation of electrodes within the limited area on an orthopedic

implant. Without losing generality and based on the structure of a mid-sized knee implant, the available area on an orthopedic implant for an Ortho-tag is assumed to be a rectangle area with a dimension of  $W$  by  $H$ .

#### **4.3.1.1 The objective function**

As preliminary work in section 2.5 has shown that large electrodes have less signal attenuation through tissue, electrodes in a rectangular shape are considered as the electrodes on the Ortho-tag because they fill up the corner of the constrained rectangular area for larger current conduction. However, the distance between the electrodes also affects the efficiency as a large distance between the electrodes results in small signal attenuations. The two inner borders of the electrodes use a round shape to increase the effective distance. The design of the electrodes then combines the advantages for rectangular electrodes and round electrodes and can be optimized through HFSS. The area of electrodes, from the aspect of power reception, is proportional to the current capacity of the electrodes, which can be represented in terms of short circuit current  $I_{SH}$ , as one term to calculate the transmitted power. The distance between the electrodes can be linked using the open circuit voltage  $V_{OP}$ , because the voltage is calculated from integration of the electric field strength along a path between the electrodes. The objective function in the electrode optimization is then to maximize the available power to the interior electrodes, defined as multiplication of  $V_{OP}$  by  $I_{SH}$ , given a fixed amount of power from the input.

The pattern of electrodes is shown in figure 27, where three parameters including  $D_1$ ,  $D_2$  and  $D_3$  are control parameters relating with the distance between the electrodes and the size and the shape of electrodes respectively.

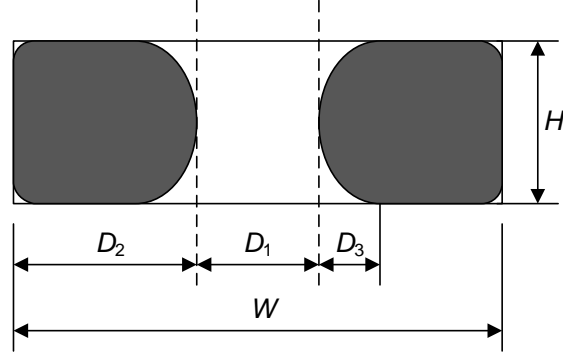


**Figure 27.** Proposed Ortho-tag electrodes

The constraint on the tag dimension is straight-forward:  $D_3$  must be less than  $D_2$  and the width of tag is  $W$ . The height and width of the electrodes are set to be the maximum  $H$  and  $W$  in order to increase the size of the electrodes. The object function is defined as follows:

$$\begin{aligned} & \text{MAX}_{D_1, D_2, D_3} \{ P = V_{OP} I_{SH} \} \\ & \text{s.t.} \quad D_1 + 2D_2 = W \quad \text{and} \quad D_3 \leq D_2 \end{aligned} \quad (10)$$

The creation of the round curved border of the electrodes is defined in figure 28 for two cases of  $D_3 \leq \frac{H}{2}$  and  $D_3 > \frac{H}{2}$  respectively. For the first case, the center of the curve is located on the horizontal line in the middle of electrodes and for the second case, the center is located at the line perpendicular to the horizontal line specified.

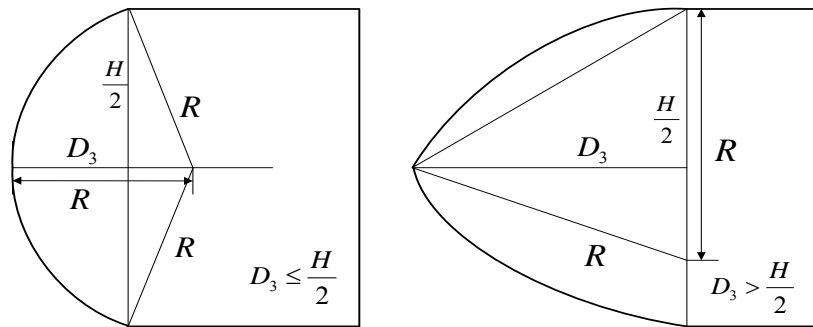


**Figure 28.** Creation of the inner border of electrodes

The radius of the inner border can be calculated from (12), by solving (11).

$$\begin{cases} (R - D_3)^2 + \left(\frac{H}{2}\right)^2 = R^2 & D_3 \leq \frac{H}{2} \\ \left(R - \frac{H}{2}\right)^2 + D_3^2 = R^2 & D_3 > \frac{H}{2} \end{cases}, \quad (11)$$

$$R = \begin{cases} \frac{H^2 + 4D_3^2}{8D_3} & D_3 \leq \frac{H}{2} \\ \frac{H^2 + 4D_3^2}{8H} & D_3 > \frac{H}{2} \end{cases}. \quad (12)$$

#### 4.3.1.2 Optimization methodology

To solve equation (10), a dimensional sweep must be performed as there is no tissue model that can be used to derive an analytical description for the power  $P$  in terms of the dimensions  $D_i$ . For a given constraint on the width of the Ortho-tag, the actual parameters that control the power are  $D_1$  and  $D_3$ , because  $D_2$  is a function of  $D_1$  within the width constraint. The given problem can be solved using the following steps. First of all, select a set of discrete values for  $D_1$  and  $D_3$  within a certain range as the input dimensions of the electrodes. Second, for each set of  $D_1$  and  $D_3$ , modify the 3D structure in HFSS and perform a field analysis for  $Z$  parameters. Third, for each set of  $D_1$  and  $D_3$ , calculate the power in (10) using the method and equations discussed in the next paragraph. Lastly, find the maximum power from the power values calculated in the third step and use the set of  $D_1$ ,  $D_2$  and  $D_3$  that has the maximum  $P$  as the optimal solution for the electrode dimensions. To save time and reduce the amount of work, an analysis with a rough range of the dimensions can be performed at the beginning to seek for an accurate range. The steps are repeated within the accurate range of dimensions for the optimal solution.

The calculation of open circuit voltage and short circuit current for each set of dimensions is based on the operation of field analysis result, which cannot be obtained automatically from

HFSS. Alternatively, Z-parameters are used in the calculation of  $V_{OP}$  and  $I_{SH}$  by adding two ports at both source and load. From equation (3), for a given  $V_S$ , setting  $I_L$  to 0, one can get equation (13) for  $V_{OP}$  using Z-parameters:

$$V_{OP} = \frac{Z_{21}}{Z_{11}} V_S, \quad (14)$$

Similarly, by setting  $V_L$  to 0, one can calculate the short circuit current using equation (15).

$$I_{SH} = \frac{Z_{21}}{Z_{12}Z_{21} - Z_{11}Z_{22}} V_S, \quad (15)$$

The normalized power in equation (16) in terms of Z-parameters is then used in the optimization process.

$$P_N = \frac{Z_{21}^2}{Z_{11}(Z_{12}Z_{21} - Z_{11}Z_{22})} \quad (16)$$

### 4.3.2 Matching network optimization

This section details the methodology for optimizing the matching networks. Section 4.3.2.1 introduces and discusses the methodology in this work on the calculation of the optimal impedances for both external and internal side of the Ortho-tag RFID system to maximize power transmission efficiency. Section 4.3.2.1 then contains the technique for the matching circuit design for the touch probe and the tag.

#### 4.3.2.1 Impedance calculation

Based on the previous discussions and according to the maximum power transfer theorem, complex conjugate matching [64] is the method of matching the Ortho-tag RFID system. The aim

of the matching network design is to match the RFID device to the conjugate value of the impedance seen from the interior electrodes, as well as match the impedance of the exterior electrodes to the impedance of the reader, normally 50 ohm. However, the impedance of the exterior electrodes and interior electrodes affect each other through their relationship to the load impedance, and the optimal impedance values cannot be derived separately. Therefore, the following steps are executed for optimal values of the optimal load impedance and the impedance from the electrodes.

The impedance calculation in this work is based on the assumption that the matching networks are passive, including only inductors and capacitors, whose power consumption can be negligible compared to that of the RFID chip. Therefore in the calculation, the power of load is assumed to be equal to the power of the RFID chip and maximization of the load power is to maximize the chip power. The key point is then to find out an expression for the load power  $P_L$  in terms of the load impedance  $Z_L$  as the objective function. In the Ortho-tag RFID system, the output power from the reader is then considered as a constant  $P_{RD}$ , which is maximized through matching the external side of tissue to the reader. The power  $P_{RD}$  is then assumed equal to the power transmitted to the tissue from port 1 in figure 26.

$$P_{RD} = |I_S|^2 R_S = |I_S|^2 \text{Re}(Z_S). \quad (17)$$

The voltage across the exterior electrodes, using equations (2) and (17), can be then written as:

$$|V_S| = |I_S| |Z_S| = |\varphi_1(Z_L)| \sqrt{\frac{P_{RD}}{\text{Re}[\varphi_1(Z_L)]}}. \quad (18)$$

From equations (2) and (18), the voltage across the load is:

$$|V_L| = |\varphi_2(Z_L)| |V_S| = |\varphi_1(Z_L)| |\varphi_2(Z_L)| \sqrt{\frac{P_{RD}}{\text{Re}[\varphi_1(Z_L)]}}. \quad (19)$$

The power received by the load is then

$$P_L = \left( \frac{|V_L|}{|Z_L|} \right)^2 \operatorname{Re}(Z_L) = \frac{|\varphi_1(Z_L)|^2 |\varphi_2(Z_L)|^2 \operatorname{Re}(Z_L) P_{\text{RD}}}{|Z_L|^2 \operatorname{Re}[\varphi_1(Z_L)]}. \quad (20)$$

Equation (20) is the objective function to be maximized and the load impedance  $Z_L$  is the one that is seen from the electrodes on the Ortho-tag. The optimization problem is expressed in equation (21), with real and imaginary parts of load impedance as control parameters. The two functions  $\varphi_1$  and  $\varphi_2$  are from equations (7) and (9), in which the  $Z$ -parameters are pre-set parameters from the field analysis using HFSS. Through maximizing the power in (21), the voltage across the RFID chip is also maximized.

$$\begin{aligned} \max_{R_L, X_L} \quad & \left\{ P_L = \frac{|\varphi_1(Z_L)|^2 |\varphi_2(Z_L)|^2 \operatorname{Re}(Z_L)}{|Z_L|^2 \operatorname{Re}[\varphi_1(Z_L)]} \right\} \\ \text{s.t.} \quad & R_L > 0, X_L > 0, Z_L = R_L + jX_L \end{aligned} \quad (21)$$

The solution of equation (21) can be obtained using the gradient descent method in which  $Z_L$  is updated from the following equation;

$$Z_L^{(n+1)} = Z_L^{(n)} - \alpha \nabla P_L(Z_L), \quad (22)$$

where  $\alpha$  is the step size. The gradient of the power cannot be obtained analytically. However a numerical expression can be used from equation (23) in which  $h$  is a small variation [65].

$$\nabla P_L = \left[ \frac{P_L(R_L + h, X_L) - P_L(R_L, X_L)}{h} \quad \frac{P_L(R_L, X_L + h) - P_L(R_L, X_L)}{h} \right]^T. \quad (23)$$

Note that the solution  $Z_L^*$  is the impedance to which the RFID device should be matched whose maximum power  $P_L^*$  is the power the RFID chip can receive.  $Z_S^*$  is calculated from equation (2), which needs to be matched to the RFID reader, a 50 ohm value.

### 4.3.2.2 LC value calculation

The matching networks are designed so that the impedance from both sides of the Ortho-tag RFID system can be matched to the desired one. As from both simulation and measurement the impedance seen from the exterior electrodes is capacitive, the LC value for the matching network in figure 16(a) on the touch probe of the HF system can be determined as follows;

$$\begin{cases} L = \frac{5\sqrt{2}\sqrt{R_s^{*3} - 50R_s^{*2} + R_s^*X_s^{*2}} + 50X_s^*}{\omega(R_s^* - 50)} \\ C = \frac{R_s^*}{\omega 5\sqrt{2}\sqrt{R_s^{*3} - 50R_s^{*2} + R_s^*X_s^{*2}}} \end{cases}, \quad (24)$$

where  $R_s^*$  and  $X_s^*$  are real and imaginary parts of  $Z_s^*$ . The copper bar does not only link the matching circuit to the electrodes, it is also a part of the inductance in the circuit. The  $L$  value is then the equivalent inductance of the combination of the copper bar and the IC inductor.

As to the HF Ortho-tag whose matching network uses figure 18(a), because there are three components in the matching circuit to adjust the impedance, one component must be fixed before figuring out the rest two. The inductor then becomes the one needed to be determined at the beginning considering the availability of parts. Assuming its inductance is given which combines the impedance of the RFID chip into  $Z_C' = R_C' + jX_C'$ , the matching network should satisfy the following equation;

$$R_L^* - jX_L^* = \frac{X_2'^2 R_C'}{R_C' + (X_2 + X_C')^2} + jX_1 + j \frac{X_2 (R_C'^2 + X_2 X_C' + X_C'^2)}{R_C'^2 + (X_2 + X_C')^2}, \quad (25)$$

where  $R_L^*$  and  $X_L^*$  are real and imaginary parts of  $Z_L^*$ , and  $X_1$  and  $X_2$  are the impedance of capacitors  $C_1$  and  $C_2$  in figure 18(a).

Equation (25) leads to the solution of the capacitance of  $X_1$  and  $X_2$ , from which capacitors  $C_1$  and  $C_2$  can be calculated.

$$\begin{cases} X_1 = -X_L^* - \frac{X_2(R_C'^2 + X_2X_C' + X_C'^2)}{R_C'^2 + (X_2 + X_C')^2} \\ X_2 = \frac{-X_C'X_L^* \pm \sqrt{R_L^*R_C'(X_C'^2 - R_C'R_L^* + R_C'^2)}}{R_L^* - R_C'} \end{cases} \quad (26)$$

In equation (26),  $\sqrt{R_L^*R_C'(X_C'^2 - R_C'R_L^* + R_C'^2)}$  is always satisfactory, and the sign is determined by making both  $X_1 < 0$  and  $X_2 < 0$ .

Because of the limitation of space on the Ortho-tag, all components in the matching network use components with a shielded surface mount package.

#### 4.4 UHF SYSTEM OPTIMIZATION

Different from the optimization method for the HF system, the inductance of the matching circuit for the UHF system relies on the wire conductor pattern on tag, because UHF frequencies are high enough to form a large inductance even with a small piece of wire. Because of the lack of feasible model representing the relationship between the wire pattern and its impedance, the optimization purely relies on the simulation using HFSS, from which the inductance of wire pattern can be determined from Z-parameters and can be observed from ports defined within the structure.

##### 4.4.1 UHF touch probe optimization

The touch probe uses rectangular electrodes instead of round as indicated in figure 15 for correspondence with the UHF tag and for the ease of design. The optimization for the UHF

touch probe follows the same principle except that the UHF touch probe has an additional capacitor  $C_S$  in series with the inductor to control the overall inductance in series with the circuit as shown in figure 16(b). The inductance and capacitance can be obtained using equation (24) with  $C$  in the second equation substituted by  $C_P$ . However, the inductance in the circuits is formed purely by the pattern of the conductor, a straight trace in this work. Therefore the optimization of the matching circuit is based on HFSS simulation for its impedance whose procedure is introduced in the following paragraph.

Due to the fact that even a small piece of wire or conductor results in a large impedance at UHF frequencies, analyzing the inductance of the wire conductor may cause a huge error because the redundant impedance connecting the wire to a port is not negligible. A better way to match the touch probe and avoid directly computing the impedance of the conducting trace is then to tune the two capacitors  $C_S$  and  $C_P$  with the length of inductor trace fixed and observe the overall impedance seen from the input port. The length of trace is then first adjusted so that the electrodes on the touch probe have enough space to provide a relatively large tolerance for misalignment. The control parameters for the optimization of the touch probe matching network then become  $C_S$  and  $C_P$ , with the impedance from input port matched to 50 ohm (the reader) as a goal. However, the relationship between the capacitors and the input impedance from the touch probe cannot be expressed analytically due to absence of expression for the inductor; a matching chart must be created with respect to the two capacitors (figure 29 and figure 30) after performing simulations and analyzing the input impedance with various sets of capacitor values. In the matching chart, the red lines are contour of reactance of the port impedance and the blue lines represent the resistances. The optimal values for the capacitors are then the intersection of two lines with the specific matched values as indicated in figure 30.

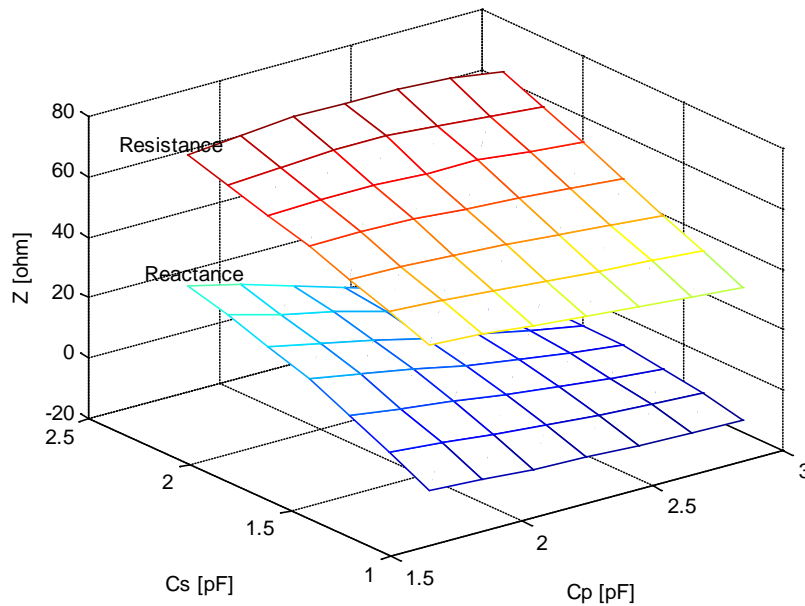


**Figure 29.** Touch probe impedance changes vs.  $C_s$  and  $C_p$

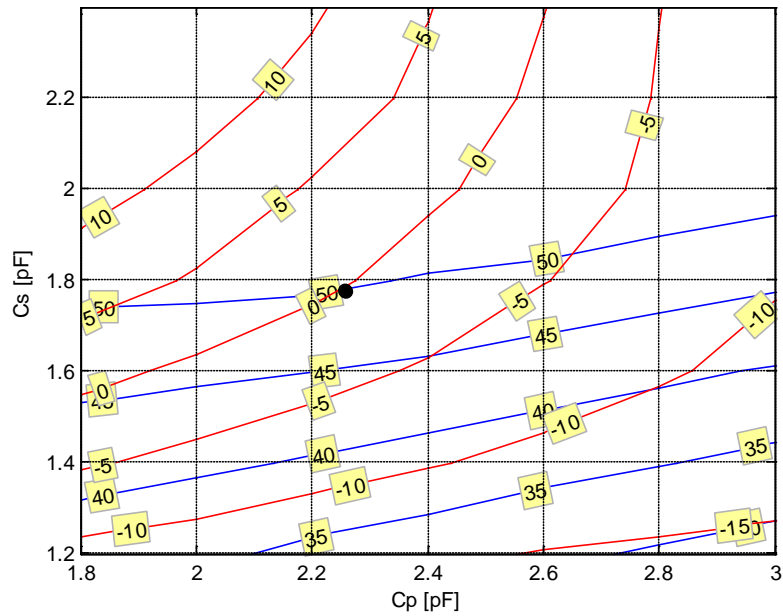


**Figure 30.** The matching chart for the UHF touch probe; resistance lines are in blue and reactance lines are in red

The solution for the capacitors can be found from the matching chart in which the real part and the imaginary part of the impedance that the touch probe is matched to are represented by a separate line. Each line represents a fixed value indicating what the touch probe is matched

to with a relationship between  $C_s$  and  $C_p$ . Therefore, for the objective impedance, the solution is the intersection point of the two lines representing the real and imaginary part of that impedance.

#### 4.4.2 UHF Ortho-tag optimization

The optimization for the UHF Ortho-tag combines the matching network design with the electrode optimization. This is because at UHF, separation of the mentioned two parts will introduce a connection conductor for each impedance simulation which is unnecessary in the design but can cause a large error. The electrodes of the UHF tag are selected as rectangular shape for two main reasons. First, a rectangular shape has larger area within the given rectangular constrained area. Second, the use of rectangular shape in electrodes can reduce the design complexity to reduce time in simulation because there is no need to optimize curvature.

The matching network for the UHF Ortho-tag uses the same technology as for its touch probe in simulation except that the capacitance on tag is formed by meander-line wire as shown in figure 17(b). The impedance of the matching wire is determined by its length, width and the space between two vertical lines. The objective function is to match the impedance seen from the matching network to the chip impedance (equation 27) using conjugate matching. Setting the space to be equal to the width of the wire, the control parameters are then further reduced to two (figure 31). A matching chart is also obtained in figure 32 and figure 33.

$$\begin{aligned} \text{MIN}_{s,w,D_1} \quad & |Z - Z_c^*| \\ \text{s.b.} \quad & s = w \quad \text{and} \quad D_1 \leq W \end{aligned} \quad (27)$$

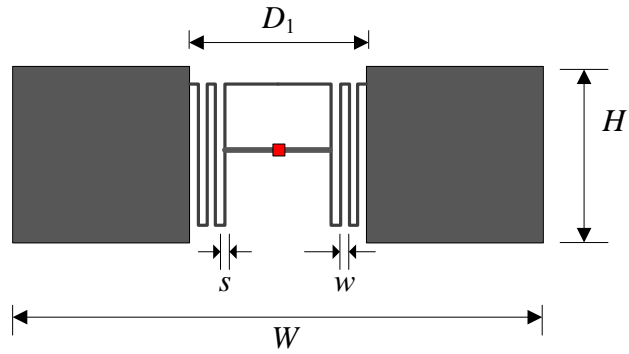


**Figure 31.** The control parameters for the UHF matching network

The observation port is at the red rectangle where the RFID chip is placed. The port impedance is then matched to the RFID chip through adjusting  $s$  and  $D_1$ . With a given range of  $w$  from 0.1 mm to 0.4 mm and a given range of  $D_1$  from 8 mm to 12 mm, the matching charts are shown in the following figures.

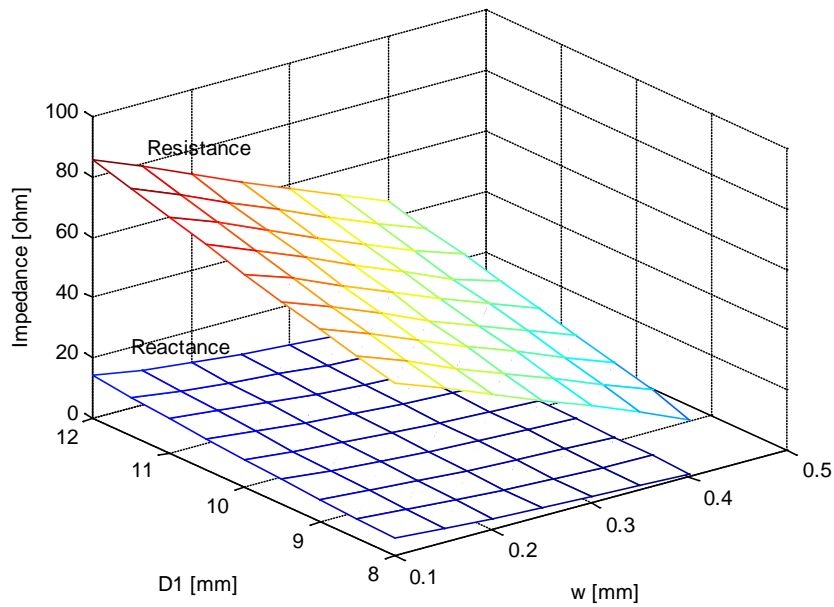


**Figure 32.** UHF Ortho-tag impedance changes vs.  $w$  and  $D_1$

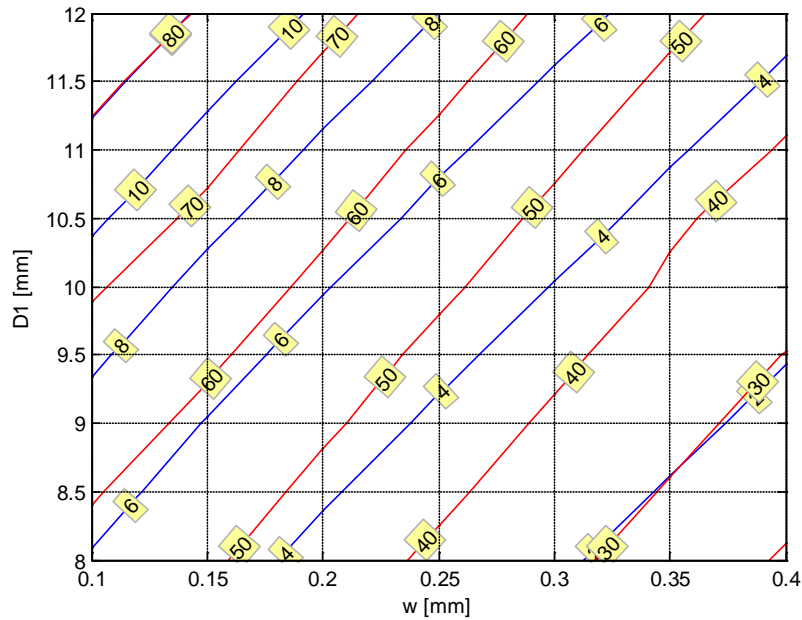


**Figure 33.** UHF Ortho-tag matching chart

#### 4.5 THE DESIGN FLOW

The design flow for optimizing the Ortho-tag RFID system is shown in figure 34. The first step is the optimization of the electrodes for which the Z-parameters can be analyzed through field analysis by HFSS. The field analysis is then a power maximization process performed based on a small range of discrete tag dimensions including its size and the distance between electrodes. The Z-parameters for the optimized electrodes are analyzed and calculated by adding two ports with one at the external side of the system and the other at the internal side. With the Z-parameters from field analysis, the optimal impedance is calculated for maximizing the power transmission efficiency. The components in the matching networks can be calculated and determined from the optimal impedance. The optimization of the matching network is then performed through field

analysis for accuracy with minor adjustment to the values of the components so that they are optimized with the wires connecting them. Analysis sweeping of the lumped parameter values or dimensions of the meander line matching network using HFSS is performed with the values within a small variation of the values from calculation. Maximum power and the corresponding values of the components are selected as the final optimal solution for the matching networks. The final step is to verify the Ortho-tag RFID system and perform necessary turning operations on the matching network.

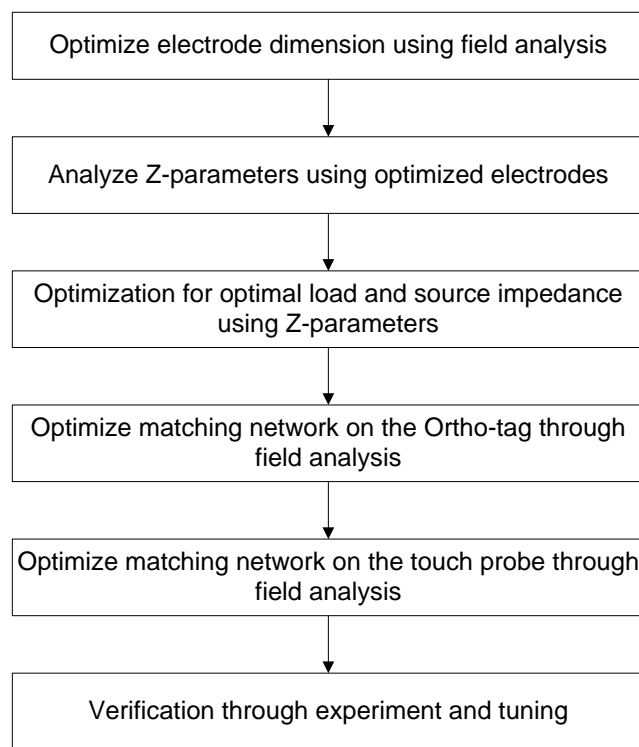


**Figure 34.** The design flow for optimizing the Ortho-tag RFID system

## **5.0 PROTOTYPE AND VERIFICATION**

This chapter discusses the prototyping of the proposed Ortho-tag RFID system, including the touch probe and Ortho-tag for both HF and UHF systems. The aim of this chapter is to demonstrate the feasibility and rationality of the proposed system and its optimization method. For verification purposes, each system is tested by reading an Ortho-tag through pig skin with the reading range in terms of thickness/layers of the pig skin. The impedances of the touch probe and the Ortho-tag in the tests are measured using a network analyzer and compared with the simulation results for error analysis.

### **5.1 HF ORTHO-TAG RFID SYSTEM**

The simulation of the HF Ortho-tag RFID system is performed on HFSS, with Z parameters of tissue being adjusted as shown below. The parameters that are obtained from simulation for the matching networks are in table 1.

One thing must be pointed out is in the simulation, the tissue parameters originally follow the wet skin parameters from [60], whose parameters are for the human tissue measured at 37 °C. In the experiment, pig skins are used as a demonstration for tissue and the temperature is kept at the room temperature, around 22 °C. The difference in the temperature has led to large differences in the conductivity of tissue as tissue tends to be more conductive at higher

temperatures [66, 67, 68]. Another factor that affects the efficiency is the electrode-tissue interface contact [39] which in the simulation is set to be an ideal case with full contact but not achievable in practice. In order to obtain a better simulation result to match the measurement in experiment with pig skin, the conductivity is adjusted to 1/5 of that from [60] for simulation so that the conductivity in simulation is close to that observed from experiments.

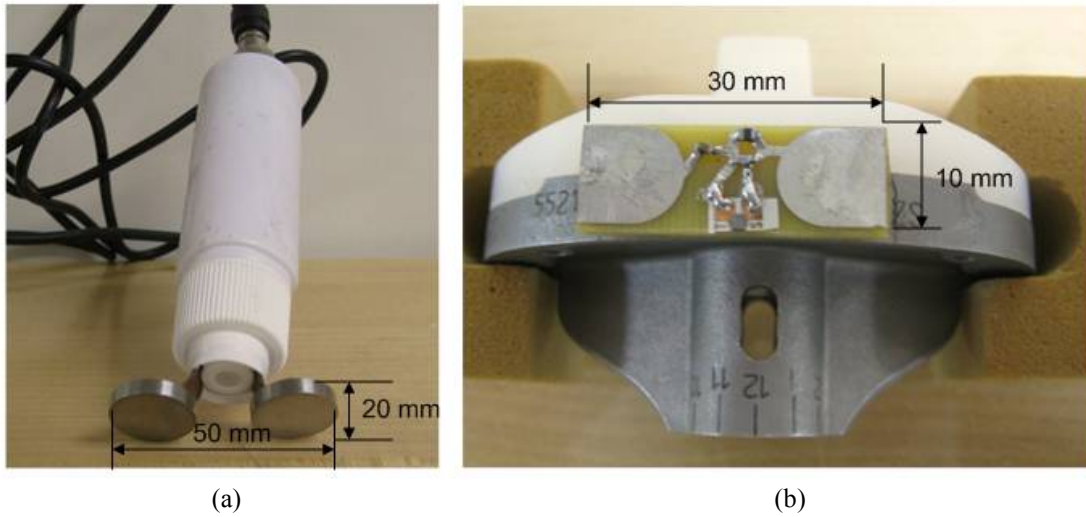


**Figure 35.** (a) HF touch probe and (b) the HF Ortho-tag

The prototype HF Ortho-tag RFID system uses the Magellan Mars-2 reader and its RFID chip. The touch probe is optimized to have two round electrodes with 20 mm diameter and 4 mm in thick. The distance between the electrodes on the touch probe is adjustable by bending the copper bars, within a range from 10 mm to 12 mm. The optimized Ortho-tag has a dimension of 30 mm by 10 mm with parameters  $D_1$ ,  $D_2$  and  $D_3$  in figure 27 being equal to 9 mm, 10.5 mm and 5 mm respectively. Using a matching network with an inductor of 1.0  $\mu\text{H}$  and capacitor of 180 pF, the touch probe is matched to  $54.6 + j4.8$  ohm, close to that of the reader. The values of L, C1 and C2 on the Ortho-tag are 1.5  $\mu\text{H}$ , 24 pF and 64 pF respectively. The S11 and parameter from the measurement and simulation are shown in figure 36.

**Table 1.** Impedance from simulation and measurements for the HF system

<b>Name</b>	<b>Value</b>
Z11 from simulation	132.69 -j28.422
Z12 from simulation	6.0543 - j2.0002
Z22 from simulation	179.73 - j52.553
Z11 from measurement	121 – j41 ohm
Z22 from measurement	202.7 – j85.3 ohm
Touch probe matched to	54.6 + j4.8 ohm
Tag matched to	189 + j92 ohm

As for the range of operation, the number of pig skin layers that can be read through is the parameter that has been recorded. With an average thickness of 4 mm pig skin, through the number of layers, one can estimate the effective operation range of the Ortho-tag RFID system. With approximately 3.3 W of power from the reader, the reading range is shown in table 2. The reading efficiency is defined as in equation (28) with a total number of 20 reading attempts.

The reading efficiency, defined as the successful rate of the read operation through different thickness of pig skins (equation (28)), is in relation to the power and signal transmission efficiency. However, a large reading efficiency does not only mean high power transmission efficiency, but it also indicates how well the touch probe needs to be aligned with the Ortho-tag in order to make it work. As will be discussed in the next chapter, misalignment of the touch probe can cause a 25 % efficiency loss, thus reducing the reading successful rate. Generally speaking, a high reading efficiency means large tolerance in the touch probe alignment while a low reading efficiency requires the well alignment of the touch probe.

$$\text{Reading efficiency} = \frac{\text{Number of successful reading times}}{\text{Total number of reading times}} \quad (28)$$

**Table 2.** Reading range for the HF system

Pig skin layer	Reading Efficiency (Matched)	Reading Efficiency (Un-matched)
1	100 %	100 %
2	100 %	70 %
3	100 %	15 %
4	60 %	0
5	20 %	0
6	10 %	0
7	0	0

## **5.2 UHF ORTHO-TAG RFID SYSTEM**

At UHF frequencies, the temperature has less impact on the conductivity of tissue as well as the electrode-tissue interface because UHF wave is more penetrating. When the wavelength becomes small enough, the transmission does not only rely on the movement of ions in tissue but also the EM waves. The simulation and experimental results are matched better than the HF Ortho-tag system when using the tissue parameters including conductivity and permittivity from [60].

The prototype UHF Ortho-tag RFID system uses the SAMSys reader and the TI inlay chip. The touch probe is optimized to have two rectangular electrodes with 16.7 mm by 15 mm. The electrodes have a thickness of 5 mm. The distance between the electrodes is fixed to be 16.6 mm by using a PCB. The inductor length is 17 mm with an additional 3 mm trace that connects

the matching circuit. An SMA adapter is used to connect the matching network to the reader through a 50 ohm coaxial cable as shown in figure 15(b). The parameters listed below are based on the following port definition. Port 1 is defined as the input port from the reader which is to be matched to 50 ohm, and port 2 is defined as the load that needs to be matched to the RFID chip.

**Table 3.** Impedance from simulation and measurements for the UHF system

Name	Value
Z11 from simulation	$50.9 + j1.25$ ohm
Z22 from simulation	$6.0 + j58.2$ ohm
Z11 from measurement	$54.2 + j4.7$ ohm
Z22 from measurement	$5.7 + j65.2$ ohm

The prototype UHF Ortho-tag and its touch probe are in figure 36.

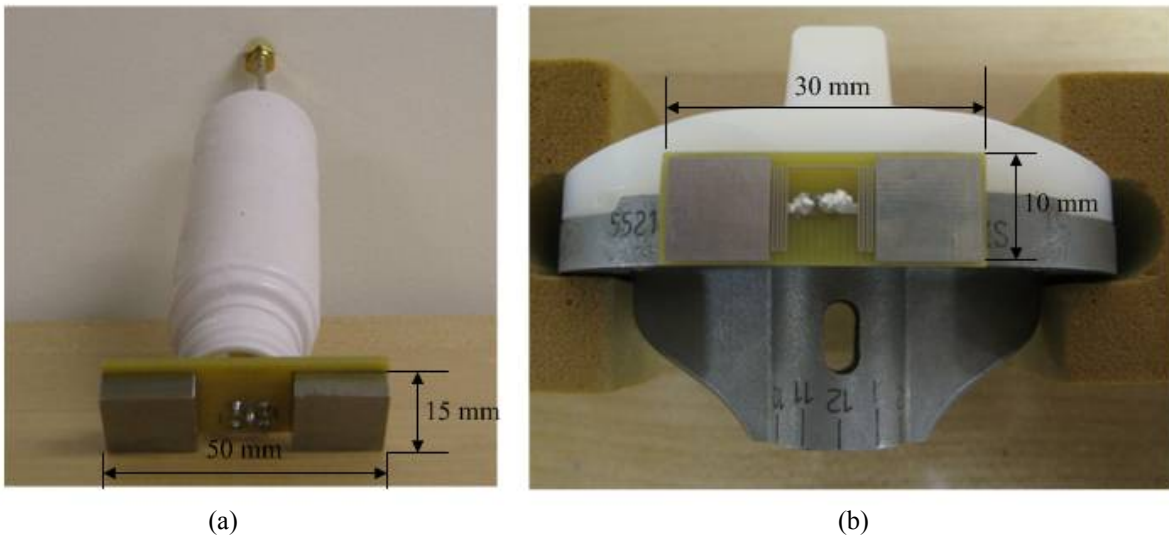


**Figure 36.** (a) UHF touch probe and (b) the UHF Ortho-tag

The read range is shown in table 4, with the same definition of reading efficiency as in equation (28). For each number of pig skin layers, the total reading time is set to 20. Because at UHF frequencies, power can be transmitted through RF wave reflection from the table or base,

whose path may not encounter tissue, the knee implant needs to be totally wrapped by the pig skin as in figure 37, so that all power transmitted to the tag interacts with the pig skin.

**Table 4.** Reading range for the UHF system

Pig skin layer	Reading Efficiency (Matched)	Reading Efficiency (Un-matched)
1	100 %	100 %
2	100 %	80 %
3	100 %	50 %
4	100 %	10 %
5	80 %	0
6	50 %	0
7	30%	0
8	10%	0
9	0	0



**Figure 37.** Experiment on a UHF system: knee implant wrapped by pig skin

### 5.3 ERROR ANALYSIS

This section discusses the factors that generate errors between the experimental results and simulation, especially in the  $Z$  matrix and matching. Major factors that can cause mismatch to the matching networks as well as the whole system include the electrode-skin interface and the environmental change such as temperature and humidity. Further errors include impedance and noise introduced by silver epoxy which is used in the prototype Ortho-tag to tie the RFID chip to the tag.

#### 5.3.1 Electrode-skin interface impedance

One issue in the area of electrode connections is the conversion of ionic tissue current to electrical current in the Ortho-tag, and vice versa. A replacement of the charge carrier from conduction electron in the metal electrode to ion in the tissue must occur at the electrode-tissue interface, a consideration of the electrochemistry, and its relationship to electrode material and shape is important [69, 70]. Control of the potential and charge transfer at this interface has a profound effect on how well the implant coexists with the contacting tissue. Based on such considerations, the majority of commercial electrodes have special coatings such as gold coating introduced in section 3.3.3 to reduce the interface impedance. However, in the experiments, copper is used for the electrodes which causes an increase in the measured impedance.

Furthermore, in the HFSS simulation, the conversion from tissue current to electrical current in metal is assumed to be ideal, which ignores the impedance from electrical transition between tissue and the electrodes. The tissue is also modeled as an electrical material without considering its conductivity limit. However, the electrode-tissue interface introduces impedance

to both the external side and internal side in practice, causing a difference between measurement and simulation. The idealization of the electrode-skin contact in simulation therefore results in smaller impedance values in the  $Z$  matrix compared with the measurements. Additionally, the simulation assumes that the electrodes have full contact with the tissue which is difficult or even impossible to be satisfied in the experiments because tissue is not perfectly flat to eliminate the small gaps between the tissue and the electrodes which also contribute to the increase in the measured impedance.

Another factor that causes mismatching and efficiency reduction is the skin to skin interface impedance, especially existing when multiple layers of pig skins are used by placing one layer on top of the other to form thick tissue. A force is added by hand through the touch probe on the skins so that each layer has a good contact with adjacent layers. Due to the fact that pig skin is not perfectly flat or perfectly connected, a number of gaps between the layers may occur to cause an impedance increase. As the number of layers increase, the skin-to-skin interface impedance accumulates and becomes greater making the parameters in the measured  $Z$  matrix increase. This is also one of the reasons why the matching for the Ortho-tag systems is designed based on 8 mm tissue, an equivalent of two layers of pig skin.

### **5.3.2 Temperature and humidity**

According to [66], temperature can affect tissue conductivity and therefore affects the  $Z$  parameters and power transmission efficiency. This is also true in the experiments in this work where the observed impedance doubled when the pig skin was cold. At high temperatures, ions in tissue become more active which in turns results in a low impedance while at a low temperature a larger impedance is observed. The change of impedance with temperature requires that the

measurements are performed in an environment with constant temperature. In the experiments, the pig skins are kept in warm water for at least 20 minutes before experiments in order to make sure their temperature is close to that of the room temperature. However, this process does not guarantee that the temperature of pig skin is evenly distributed which in turn causes an increase in the measured impedance and mismatching. The temperature effect in the UHF system is not as big as in the HF system and therefore the difference between measurement and simulation is much smaller for the UHF system.

Because water increases the fluidity of ions in tissue, human tissue containing more water tends to have more ions to conduct electricity than dry tissue and thus has a smaller resistance. From the electrical features of human skin at HF [60], wet skin has almost 150% conductivity of that of dry skin. Therefore, in a humid environment the human tissue dehydration process is slow and this keeps the tissue at a low impedance for a long period of time. However, in a dry environment, dehydration is much faster and causes a fast change in impedance of tissue. There is no severe difference for the conductivity between dry skin and wet skin at UHF frequencies according to [60] because at UHF ions is not the only manner to transmit power.

### **5.3.3 Other factors**

Other considerations include the use of silver epoxy for connecting the RFID chip to the Ortho-tag and the traces on the HF matching circuit. The major reason for using silver epoxy is that the silver epoxy provides a strong bond as well as a good conductivity between the tag and the chip. However, due to the size of the silver epoxy on the tag being as wide as the wire trace but has a much greater thickness, it increases a large stray capacitance across the chip. This stray capacitor in turn reduces the impedance of the chip and therefore can cause a small variation on the

impedance value of the matching network. Wire bonding can be applied for the connection in the future work to reduce stray capacitance.

Another issue that affects the matching impedance is the trace in the matching network. For the HF Ortho-tag RFID system, because of the utilization IC components, traces of PCB are designed only for connection. Even though these traces are short enough to generate only a small self-impedance at HF, their values can be enlarged through the matching network and thus affect the matching. The LC values later must be tuned so that the impedance change introduced by the traces can be compensated.

## **6.0 DISCUSSIONS**

This chapter introduces concerns regarding the factors of Ortho-tag size and the touch probe alignment on the power transmission efficiency. Through simulation, power transmission efficiency for both HF and UHF frequencies, Ortho-tag RFID systems have been studied with tags in various sizes. The alignment of the touch probe in terms of its angle with the tag has also been discussed for comparison. The last section discusses the advantages and disadvantages between the Ortho-tag systems at the two different RFID frequencies.

### **6.1 POWER VS TAG SIZE**

Size of the tag is always a design issue especially when implanted, not only because of the availability of space, but also because of its impact on power. As in conventional wireless power transmission systems where antennas are used, large tags have better performance than smaller ones in that the coupling between the reader and the tags increases as size of tag increases. The size of Ortho-tag is important because it is determined by the power transmission efficiency. It is also important, from the design aspect, to determine the size of Ortho-tag to meet a given specification with the amount of power and operational range required. However, unlike the conventional wireless systems in which antennas are applied, it is difficult to derive an analytical expression for the coupling between the touch probe and the Ortho-tag through tissue. Thus the

power transmission efficiency is difficult to calculate. One method for solving such a problem is simulation using HFSS through which transmission parameters can be calculated numerically from finite element analysis. In the following two sections on the tag size, HFSS is used to calculate the  $Z$  matrix between the touch probe and the Ortho-tag from which the maximum power transmitted can be derived from equation (20) and equation (21).

### 6.1.1 HF Ortho-tag size

Because the Ortho-tag is limited within a 10 mm by 30 mm area, the range of sizes is selected to change from its limitation to 2 mm by 10 mm with 2 mm decrement for each dimension. The parameters of  $D_1$ ,  $D_2$  and  $D_3$  are adjusted so that they are proportional to the shrink in size. For each size, the  $Z$  parameters are analyzed and the maximum power received by the tag is calculated and converted to dBm. For comparison, the thicknesses of skin are set to be 8 mm for ordinary people and 28 mm for people with obesity. The simulation results are shown in figure 38 and figure 39 with  $W$  and  $H$  defined as in figure 27.

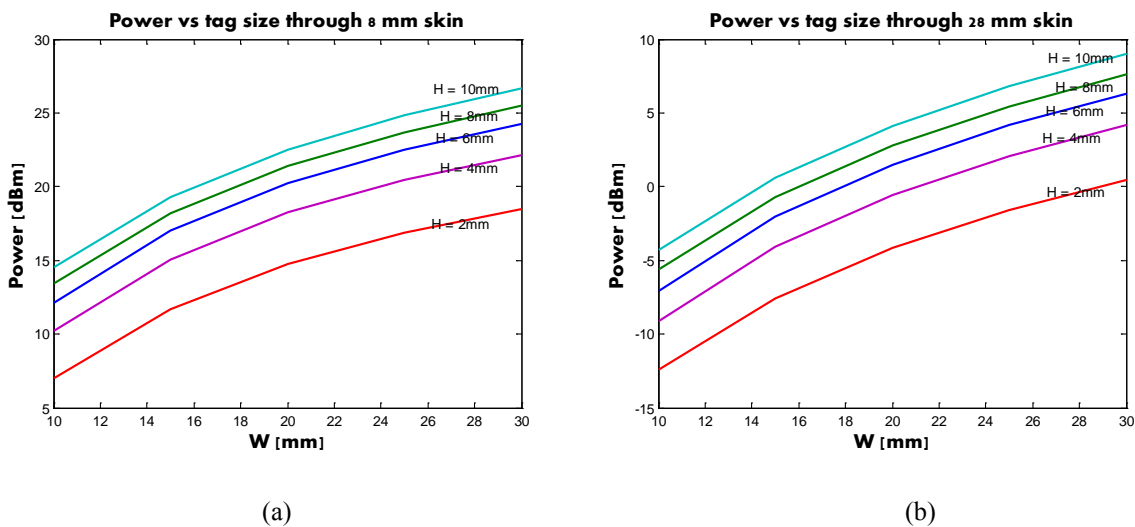
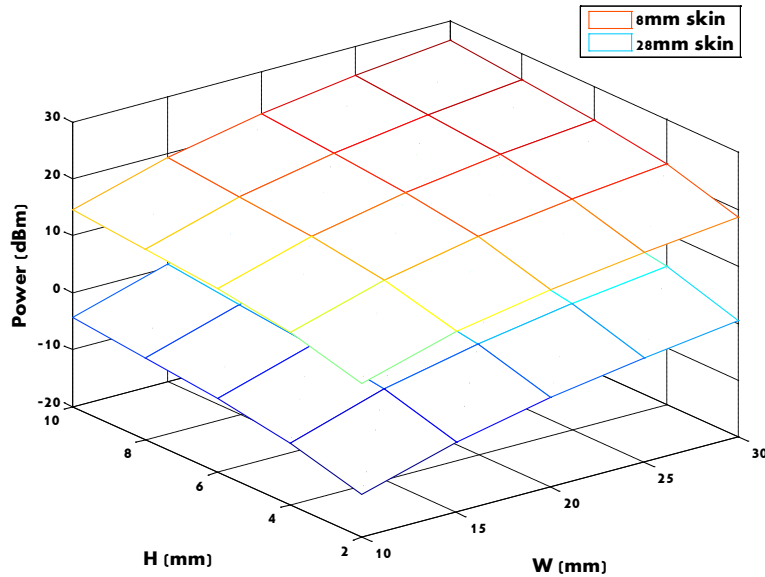


Figure 38. Power vs. tag size for HF Ortho-tag: (a) through 8 mm skin; (b) through 28 mm skin



**Figure 39.** The 3D plot for the relationship between power and HF tag dimension

The simulation results show that tag power reduces as its size is reduced. From the plots, there is approximately a linear decrease in power in dBm as the size of tag linearly reduces. The power in dBm means an exponential change when converted into power in Watts. This is in accordance with the preliminary results in the second chapter from which one finds that larger electrodes and greater distance between electrodes on the Ortho-tag result in the same trend of power increase.

The above two plots are important in that they help to determine the size of the Ortho-tag for a specific application. For example, by setting up a threshold value for the power level that is sufficient to turn on the RFID chip, one can determine whether a given size of the tag meets the design specification and therefore can find the minimum size of the Ortho-tag to be applied in a certain condition, i.e. a specific implant. Additionally, with a given size of the tag, the minimum power required to guarantee a successful read operation can be found to help designer determine if the size can be used following power regulations regarding safety concerns.

### 6.1.2 UHF Ortho-tag size

The UHF Ortho-tag in simulation uses the same table in size as that for the HF Ortho-tag.  $D_1$  is also adjusted in proportion to  $W$ , the horizontal length of tag in figure 27. Unlike in the HF Ortho-tag system where the impedance of the connection wire for the chip and the electrodes are small enough to be negligible, the wire that connects the chip port has sufficiently large impedance at UHF. Therefore, a matching capacitor following equation [71] is added to compensate the wire impedance. The simulation is also performed for both 8 mm skin and 28 mm skin.

$$C_{\text{COMP}} = \frac{1}{\omega^2 \cdot 0.00508l \left[ \ln \frac{2l}{w+h} + 0.5 + 0.2235 \frac{w+h}{l} \right]}, \quad (29)$$

where  $l$ ,  $w$  and  $h$  represent the length of wire, the width of wire and the thickness of the tag substrate. The relationship between the power and size for the UHF Ortho-tag are shown in the following two figures.

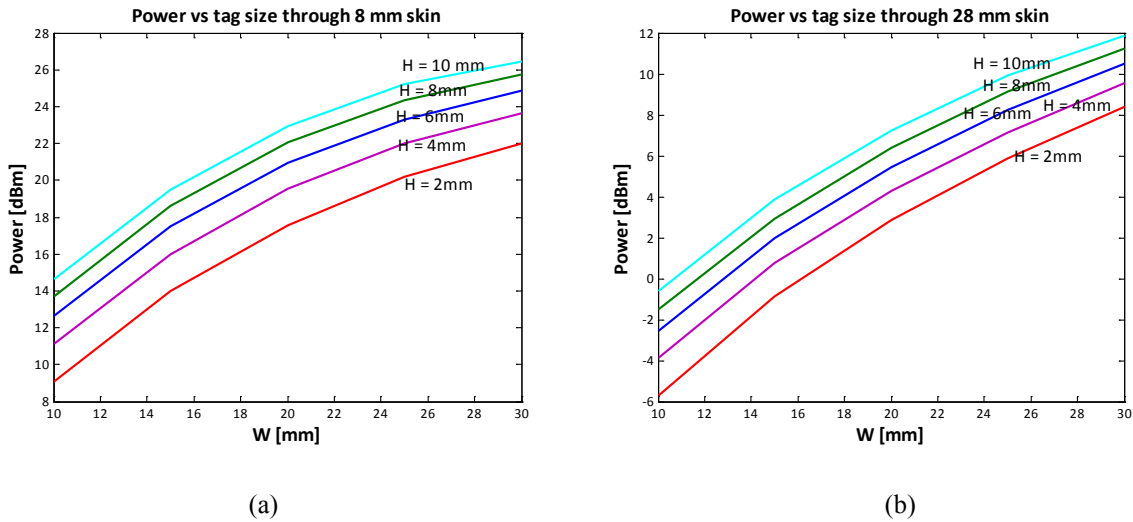


**Figure 40.** Power vs. tag size for UHF Ortho-tag: (a) through 8 mm skin; (b) through 28 mm skin

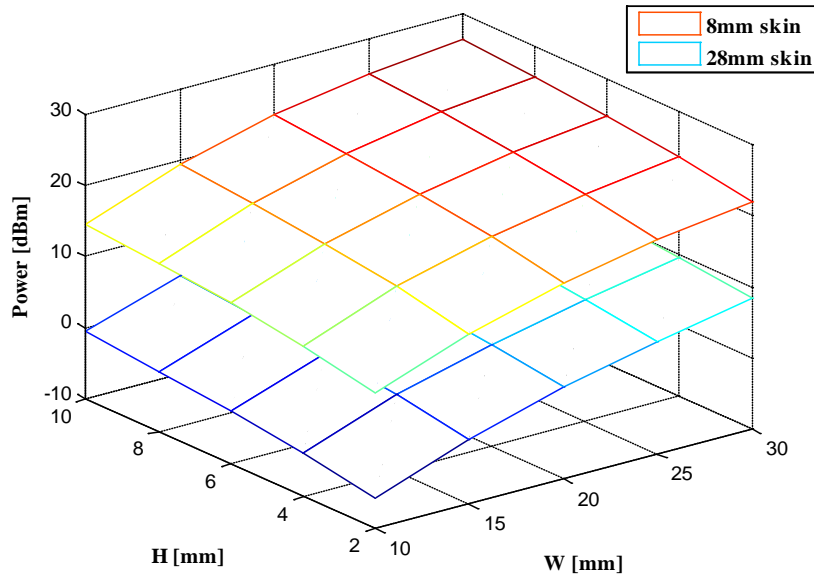


**Figure 41.** The 3D plot for the relationship between power and UHF tag dimension

## 6.2 THE POWER VS ANGLE

The location of the touch probe on tissue is another important factor that can affect the *in vivo* power transmission efficiency significantly. The Ortho-tag system requires that the touch probe well aligned with the Ortho-tag for maximum efficiency. One of the parameters that describe the touch probe alignment is its angle with the Ortho-tag. The change of angle between the touch probe and the Ortho-tag from 0 to 90 degrees can drastically change the efficiency from the maximum to the minimum. In this section, eight different locations of the touch probe are studied from simulation for both the HF system and the UHF system. Similar to previous sections, for each alignment situation, the Z matrix is computed from HFSS and the voltages at the source port and the load port are analyzed and normalized to the well aligned case.

Figure 42 shows the different situations of the touch probe alignment in which the grey pairs represent the touch probe placement and the yellow pairs represent the Ortho-tag. In the first four cases, the touch probes are only rotated to different angles but without translational movement: the axis of symmetry of the touch probe and the tag are identical. Figures 42(e) to 42(h) show the cases with touch probe rotation as well as translational movement with a distance of 40 mm between the centers of the probe and the tag. Therefore, the situations do not only cover the rotation of the touch probe precisely on top of the Ortho-tag, but also studies the cases that the probe is moved farther away, which is necessary as a guide and reference to give instructions to those who use the touch probe. Table 5 lists the voltage efficiencies defined as the ratio of voltage across the tag to that across the input port, in the different situations in figure 42. As power is in proportion to the square of the voltage, one can find that power reduces tremendously in the misaligned cases, showing that the Ortho-tag RFID system is directional whose power emitted is within a small area in tissue.

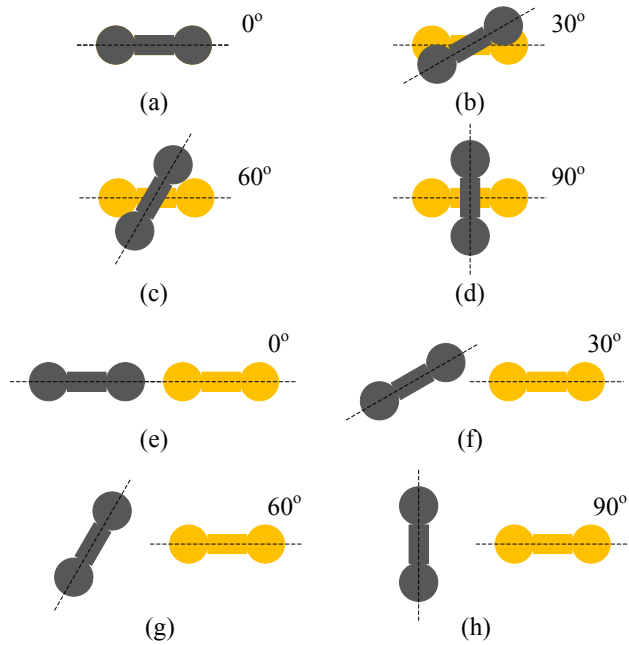


**Figure 42.** The different placements of the touch probe

**Table 5.** Voltage efficiency with different placement of touch probe (normalized to well-aligned case)

Touch Probe Placement	HF	UHF
a	100 %	100 %
b	84.5 %	87.8 %
c	46.9 %	51.4 %
d	1.17 %	3.40%
e	25.2 %	21.5%
f	19.8 %	10.0%
g	10.2%	0.80%
h	0.44%	0.54%

One thing that needs to be pointed out is that efficiency is minimized when the angle is at 90 degrees, an extreme case when the waves going into the electrodes on the Ortho-tag counteract each other. In the real operation of the Ortho-tag for a patient, a surgeon would be instructed to keep the touch probe parallel with the tag perpendicular to the vertical tibia bone and move the touch probe towards the tag for an optimum position. For a better illustration of how location affects efficiency, the efficiency vs. location of the touch probe is plotted for a radiation pattern (figure 43): the horizontal direction in the center of the plot is the direction and location of the Ortho-tag; the position of one point in the plot represents the center of the touch probe with its angle being equal to the angle of the corresponding point in the polar coordinate system. Different from a field pattern, the plots are evaluated in terms of voltage efficiency normalized to the well-aligned case with values of some points calculated from interpolation for consistency in display.

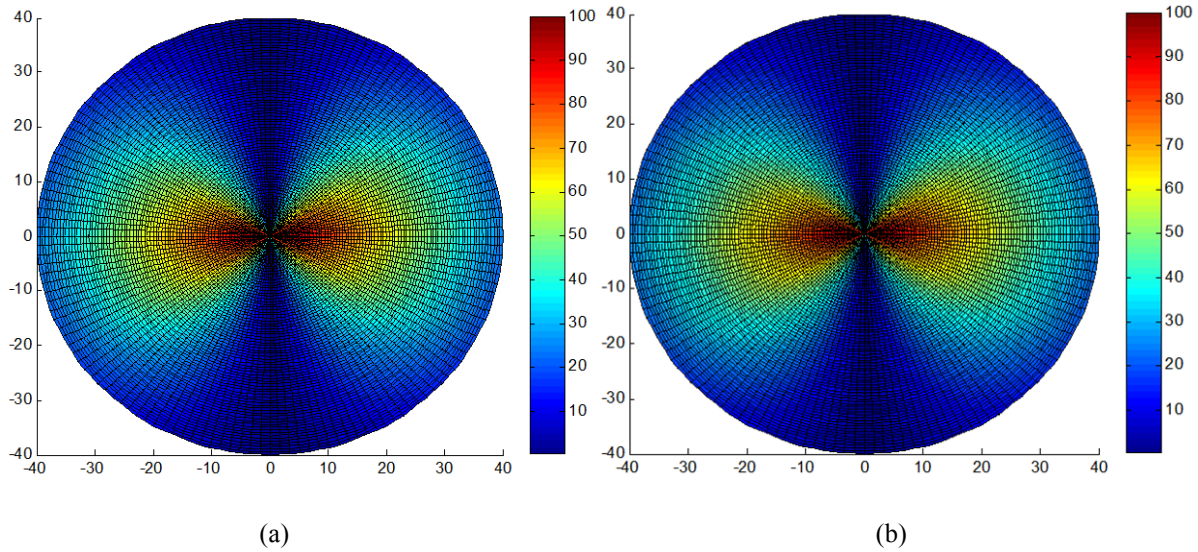


**Figure 43.** Touch probe placement vs. efficiency for HF (a) and UHF (b) systems

### 6.3 HF SYSTEM VS UHF SYSTEM

There is always a debate on the selection of the two transmission frequencies for the Ortho-tag RFID system by comparing the HF system and UHF system. Each system has its own advantages and disadvantages when used in real applications but no overwhelming benefits towards the other. As seen from the experimental results, at either frequency the Ortho-tag system can work at full efficiency when applied to two layers of pig skin, approximately 8 mm tissue which is sufficiently good for ordinary people, and the transmission range is fairly large up to around 25 – 30 mm, the comparison then focuses on the common aspects of concern such as signal attenuation, power regulation, design process, cost, compatibility and market support in the following paragraphs.

One of the major advantages for the HF system is that it has less signal attenuation through human body meaning that during the energy transmission process, a smaller portion of the power is lost in tissue. This has a positive affect on the range of transmission through tissue

considering that a large portion of the power is absorbed in human body when UHF system is applied which in turn limits the power received by the Ortho-tag. However, metallic implant interference at UHF frequencies is much smaller than that at HF frequencies, which plays a negative role over the advantage on signal attenuation at HF. Therefore, in the HF Ortho-tag system, the body absorbs less power while the implant absorbs more power than that in the UHF system, and the overall advantage in signal attenuation in the HF system is not obvious compared to the UHF system.

Due to the less power absorption condition in tissue, an HF system is potentially less harmful than the UHF system, and its limit in power and *in vivo* current specified by [51] is higher than that for the UHF system, which is another great advantage over the UHF system. Because a higher power input results in a larger range of transmission and larger tolerance in the position of the touch probe, the HF system could be beneficial for use with thick tissue in the future, such as the hip implant and people with obesity.

Fast data rate is one of the reasons people consider using UHF rather than HF, especially when reading large amount of data. With a clock frequency in the UHF range, the amount of time for reading operation is at the level of microsecond comparably smaller than that at HF at level of millisecond. To compete with the UHF in data rate, Magellan utilizes phase jitter modulation as its RFID modulation technology, and its HF system data rate achieves a considerably higher increment.

With respect to the design considerations, UHF is better than HF in the Ortho-tag design as the inductance in the matching circuit on the HF tag is difficult to form using a conductor pattern because the length of trace may exceed the size of tag. The metallic implant also acts as an inductor that performs a counter effect to reduce the inductance of the matching circuit.

Therefore, an IC inductor with shielding is used which does not only increase the design complexity but also the total cost of the Ortho-tag. The UHF Ortho-tag uses a conductor pattern to create its inductance as the value of the inductor required is much less and the orthopedic implant does not downgrade the inductance as much as that in the HF system. The UHF design does not only reduce the complexity of the matching network but also reduces the cost of tag. However, the UHF matching circuit is designed based on a matching chart from HFSS simulation; the overall time for design is much longer than the HF system because the time for HFSS to run one simulation is a couple of hours and the total amount of time for a matching chart can be several days.

Another concern for the HF and UHF systems is the environmental effects such as the temperature and humidity of the room where the reading operation is performed. From the existing literature [60] and the observation in this work, environmental change has a less impact on the UHF system than the HF system in that the conductivity change of skin is much smaller and a mismatch is less likely to be found.

Literature [24] also discusses on the interference between the RFID device and other medical devices, which points out that if another UHF device exists in another room nearby, the UHF Ortho-tag system will likely receive unnecessary signal and data. In an interference test between pacemaker and RFID signal [31], the HF RFID signal is more likely to generate interference with the pacemaker. Depending on the on-site environment, one can make a decision on the selection of operating frequency for the Ortho-tag system to avoid possible interference.

From the market aspect, the UHF RFID market is larger than that of the HF RFID market with major manufactures including ThingMagic, SAMSys and Tagsys, which is the advantage in using the UHF Ortho-tag RFID system. Furthermore, there has been existing UHF RFID chips

with high memory that can survive in harsh conditions such as in the Gamma sterilization process which is usually required before an orthopedic implant surgery is performed. Considering the development in the RFID industry, the UHF Ortho-tag RFID system will have better support from major RFID chip manufacturers.

## 7.0 CONTRIBUTION OF WORK

The major contribution of this dissertation includes the development of a volume conduction based energy transmission platform for the Ortho-tag RFID system for metallic orthopedic implant and the corresponding method on the optimization of the system. In order to increase the efficiency of the system to make it acceptable for real applications, major contributions are included in this chapter. First, this dissertation develops a method that uses HFSS to optimize the structure of the Ortho-tag electrodes including the shape and dimension of the electrodes. Second, this dissertation develops a matching method for optimizing the HF Ortho-tag impedance from the  $Z$  matrix, and realizes the optimization process in its prototype with matching networks using IC components. Third, this dissertation also optimizes the touch probe and Ortho-tag for the UHF system, through matching chart from HFSS simulation. Fourth, this dissertation discusses and compares power on tag with different sizes of tag which creates a reference for designer to determine the tag of size best fit a specific orthopedic implant. Last, from efficiency with different cases of the touch probe alignment, this dissertation proves and provides a reference for the instruction on the placement of the touch probe.

## **8.0 CONCLUSION**

This work leads to the following conclusions. First, the experiment results and the successful reading operation of the Ortho-tag demonstrate the feasibility of the proposed Ortho-tag RFID system based on volume conduction. The combination of volume conduction and RFID technology is an effective solutions to avoid metallic interference. Second, by comparing the reading efficiency between the matched system and unmatched system, this work has proven the effectiveness of its proposed method in optimizing the HF and UHF Ortho-tag system including the matching network design and the electrode optimization. Third, this dissertation also studies how the power transmission efficiency is affected by the alignment between the touch probe and the Ortho-tag whose results show that a well aligned touch probe and Ortho-tag is important in efficiency. This work also details the relationship between the tag power and size through simulation, providing an important guide for the RFID industry to design the proper size of tag for installation on a specific orthopedic implant. Finally, through comparison between the HF and UHF Ortho-tag RFID systems, this work summaries and provides a reference for the orthopedic manufactures to select the proper operating frequency that best fits their application.

## APPENDIX A

### VARIABLES DEFINED IN HFSS SIMULATION

<b>Name</b>	<b>Description</b>	<b>Value</b>
SkinThickness	Thickness of skin tissue	[8 mm, 28 mm]
Wmax	Maximum width of tag	[10 mm, 30 mm]
Hmax	Maximum height of tag	[2mm, 10 mm]
TagX	Tag center	0 mm
TagY		-19 mm
TagZ		-7 mm
TagThickness	Thickness of tag	1.54 mm
D1	These parameters follow figure 27	[6mm, 16mm]
D2		$(Wmax-D1)/2$
D3		5 mm or 0 mm
Theta	Angle of curve in figure 28	$\text{atan}(Hmax/2/D3)$
R1	Radius of curve for $D3 \leq Hmax/2$	$Hmax/D3 * Hmax/8 + D1/2$
X1	Curve center ( $D3 \leq Hmax/2$ )	$R1 - R1 * \sin(\text{Theta}) + D1/2$
Y1		$R1 * \cos(\text{Theta})$
R2	Radius of curve for $D3 > Hmax/2$	$Hmax/4 + D3^2/Hmax$
X2	Curve center( $D3 > Hmax/2$ )	$D1/2 + D3 - R2 * \sin(\text{Theta})$
Y2		$Hmax/2 - R2 + R2 * \cos(\text{Theta})$
TraceThickness	Thickness of trace on tag	0.04318 mm
Cs, Cp	Capacitor for UHF touch probe	[1.2pF, 2.4pF]
w	Width of trace on UHF Ortho-tag	[0.2mm, 0.7mm]
s	Space between trace on UHF Ortho-tag	w

## APPENDIX B

### MATLAB CODE FOR ELECTRODE OPTIMIZATION

```
% Xiaoyu Liu <xil56@pitt.edu> Ortho-tag project
% RFID Center of Excellence
% University of Pittsburgh
% Optimizing electrodes for HF Ortho-tag

clear all
clc

% DEFINE CONSTANT
FILENUMBER = 1;
SOLUTIONNUMBER = 8;
MAXPASSES = 20;
POUT = 4;
%END

ZDATA = zeros(MAXPASSES, SOLUTIONNUMBER*8+1, FILENUMBER);
Z11 = zeros(SOLUTIONNUMBER, FILENUMBER);
Z12 = zeros(SOLUTIONNUMBER, FILENUMBER);
Z21 = zeros(SOLUTIONNUMBER, FILENUMBER);
Z22 = zeros(SOLUTIONNUMBER, FILENUMBER);

ZDATA(:, :, 1) = xlsread('Ortho_tag_HF_1EOPSGD1.csv');

for i = 1:FILENUMBER

    for j = 1:SOLUTIONNUMBER          % Z11 Real
        for k = 1:MAXPASSES
            if isnan(ZDATA(k, j+1+SOLUTIONNUMBER*0, i)) == 1
                Z11(j, i) = Z11(j, i) + ZDATA(k-1, j+1+SOLUTIONNUMBER*0, i);
                break;
            end
        end
    end

    for j = 1:SOLUTIONNUMBER          % Z11 Imaginary
        for k = 1:MAXPASSES
```

```

        if isnan(ZDATA(k,j+1+SOLUTIONNUMBER*1,i)) == 1
            Z11(j,i) = Z11(j,i) + ZDATA(k-1,j+1+SOLUTIONNUMBER*1,i)*1i;
            break;
        end
    end
end

for j = 1:SOLUTIONNUMBER          % Z12 Real
    for k = 1:MAXPASSES
        if isnan(ZDATA(k,j+1+SOLUTIONNUMBER*2,i)) == 1
            Z12(j,i) = Z12(j,i) + ZDATA(k-1,j+1+SOLUTIONNUMBER*2,i);
            break;
        end
    end
end

for j = 1:SOLUTIONNUMBER          % Z12 Imaginary
    for k = 1:MAXPASSES
        if isnan(ZDATA(k,j+1+SOLUTIONNUMBER*3,i)) == 1
            Z12(j,i) = Z12(j,i) + ZDATA(k-1,j+1+SOLUTIONNUMBER*3,i)*1i;
            break;
        end
    end
end

    for j = 1:SOLUTIONNUMBER          % Z21 Real
    for k = 1:MAXPASSES
        if isnan(ZDATA(k,j+1+SOLUTIONNUMBER*4,i)) == 1
            Z21(j,i) = Z21(j,i) + ZDATA(k-1,j+1+SOLUTIONNUMBER*4,i);
            break;
        end
    end
end

for j = 1:SOLUTIONNUMBER          % Z21 Imaginary
    for k = 1:MAXPASSES
        if isnan(ZDATA(k,j+1+SOLUTIONNUMBER*5,i)) == 1
            Z21(j,i) = Z21(j,i) + ZDATA(k-1,j+1+SOLUTIONNUMBER*5,i)*1i;
            break;
        end
    end
end

for j = 1:SOLUTIONNUMBER          % Z22 Real
    for k = 1:MAXPASSES
        if isnan(ZDATA(k,j+1+SOLUTIONNUMBER*6,i)) == 1
            Z22(j,i) = Z22(j,i) + ZDATA(k-1,j+1+SOLUTIONNUMBER*6,i);
            break;
        end
    end
end

for j = 1:SOLUTIONNUMBER          % Z22 Imaginary
    for k = 1:MAXPASSES
        if isnan(ZDATA(k,j+1+SOLUTIONNUMBER*7,i)) == 1
            Z22(j,i) = Z22(j,i) + ZDATA(k-1,j+1+SOLUTIONNUMBER*7,i)*1i;

```

```

                break;
            end
        end
    end
end

end

% Define variables
D1 = 2:18;
VD = zeros(1,SOLUTIONNUMBER);
ID = zeros(1,SOLUTIONNUMBER);
PD = zeros(1,SOLUTIONNUMBER);
Vs = VD;
PDdB = PD;
% End

for i = 1:FILENUMBER      % Calculate power
    for j = 1:SOLUTIONNUMBER
        Vs(j) = sqrt(POUT/real(Z11(j,i)))*Z11(j,i);
        VD(j) = (Z12(j,i)/Z11(j,i))*abs(Vs(j));
        ID(j) = (Z12(j,i)/(Z12(j,i)*Z12(j,i)-Z11(j,i)*Z22(j,i)))*abs(Vs(j));
        PD(j) = abs(VD(j)*ID(j));
        PDdB(j) = 10*log10(abs(VD(j)*ID(j)))+30;
    end
    [i -VD(4)/ID(4)]
    hold on
    plot(D1, PD);
end
hold off

```

## APPENDIX C

### MATLAB CODE FOR LOAD IMPEDANCE OPTIMIZATION

#### C.1 CODE FOR CALCULATING TAG POWER

```
% This function calculates the load power with a given load impedance
% 'x' is the load in complex value
% 'Z' is a 2x2 impedance matrix from HFSS
% 'y' is the output load power

function y = TagPower(x,Z)

Pin = 1;
RL = x(1);
XL = x(2);
Z11 = Z(1,1);
Z12 = Z(1,2);
Z21 = Z(2,1);
Z22 = Z(2,2);

ZL = RL + 1i*XL; % load impedance

y = -abs(Z21./(ZL+Z22)).^2.*RL*Pin./real(Z11-Z12*Z21./(ZL+Z22));
```

#### C.2 CODE FOR CALCULATING LOAD IMPEDANCE

```
function [ZL P] = Optload(Z)

% 3D plot of load power vs. load impedance
RL = 0:5:500;
XL = -100:1:100;
```

```

[xp,yp] = meshgrid(RL, XL);
zp = TagPower([xp yp], Z);
meshc(xp,yp,zp);
grid on

% gradient search
N = 1000; % maximum iteration times
h = 1e-3; % step for calculating gradient
DeltaP = 1e-3; %tolerance
step = 1e6; % step for the search

% initialization
RL=0;
XL = 0;
iter = 0;

while iter <N
    % gradient
    DF_RL = (TagPower([RL+h;XL],Z) - TagPower([RL;XL],Z))/h;
    DF_XL = (TagPower([RL;XL+h],Z) - TagPower([RL;XL],Z))/h;
    % update old impedance
    RL = RL - step*DF_RL;
    XL = XL - step*DF_XL;
    iter = iter + 1;
end

ZL = RL + 1i*XL;
P = TagPower(ZL,Z);

```

## APPENDIX D

### MATLAB CODE FOR CALCULATING MATCHING NETWORK PARAMETERS FOR THE HF ORTHO-TAG

```
% This program calculates C1 and C2 for the HF matching network

clear all
clc

% define frequency 13.56 MHz
f = 13.56e6;
w = 2*pi*f;

% Optimal impedance from the interior electrodes
Rs = 202.7;
Xs = -85.3

% RFID chip impedance Cd // Rdp
Cd = 7e-12;
Rdp = 4700;

% Inductor impedance Lindp // Rindp
Lindp = 1.5489e-6;
Rindp = 2.8477e3;
Xdp = -1i*1/w/Cd;
Xindp = 1i*w*Lindp;

Zd = Rdp*Xdp/(Rdp+Xdp);
Zind = Rindp*Xindp/(Rindp+Xindp);
ZL = Zd*Zind/(Zd+Zind);

RL = real(ZL);
XL = imag(ZL);

if Rs*RL*(XL^2-RL*Rs+RL^2) <0
    X2 = 0;
    X1 = 0;
```

```

    return;
end
delta = sqrt(Rs*RL*(XL^2-RL*Rs+RL^2));

X2 = (-XL*Rs-delta)/(Rs-RL);
X1 = -Xs - X2*(RL^2+X2*XL+XL^2)/(RL^2+(X2+XL)^2);

if X1 > 0
    X2 = (-XL*Rs+delta)/(Rs-RL);
    X1 = -Xs - X2*(RL^2+X2*XL+XL^2)/(RL^2+(X2+XL)^2);
end

[X1 X2]
[-1e12/w/X1 -1e12/w/X2]

```

## APPENDIX E

### MATLAB CODE TO GENERATE THE MATCHING CHART FOR THE UHF SYSTEM

```
% This program plots the matching chart for UHF system optimization

clear all
clc

% read data
ZDATA = xlsread('Touchprobe_C_new.csv');

% define capacitor range
Cs = 1.2:0.4:2.4;
Cp = 1.2:0.4:2.4;

[xp,yp] = meshgrid(Cs, Cp);

% plot the matching chart
figure(1)
zp = ZDATA(1:4,2:5);
[C,h] = contour(xp,yp,zp,[20 25 30 35 40 45 50]);
text_handle = clabel(C,h);
set(text_handle,'BackgroundColor',[1 1 .6],...
    'Edgecolor',[.7 .7 .7]);
grid on
hold on

zp = ZDATA(1:4,6:9);
[C,h] = contour(xp,yp,zp,[-20 -15 -10 -5 0 5 10]);
text_handle = clabel(C,h);
set(text_handle,'BackgroundColor',[1 1 .6],...
    'Edgecolor',[.7 .7 .7]);
grid on
hold off

% 3D plot
figure(2)
zp = ZDATA(1:4,2:5);
mesh(xp,yp,zp);
```

```
hold on
grid on
zp = ZDATA(1:4,6:9);
mesh(xp,yp,zp);
hold off
```

## APPENDIX F

### MATLAB CODE FOR PLOTTING TAG SIZE VS POWER

```
% This program plots the relationship between tag power and tag size

clear all

% DEFINE CONSTANT
FILENUMBER = 1;
SOLUTIONNUMBER = 25;
MAXPASSES = 30;
POUT = 3;
%END

DATA = xlsread('UHF_Zpara_vsize_skin08.csv');
ZDATA = zeros(MAXPASSES,SOLUTIONNUMBER*8+1,FILENUMBER);
Z11 = zeros(SOLUTIONNUMBER, FILENUMBER);
Z12 = zeros(SOLUTIONNUMBER, FILENUMBER);
Z22 = zeros(SOLUTIONNUMBER, FILENUMBER);

for i = 1:FILENUMBER
    Z11_R1 = 2+SOLUTIONNUMBER*(i-1);
    Z11_R2 = Z11_R1+SOLUTIONNUMBER-1;
    Z11_I1 = Z11_R1+SOLUTIONNUMBER*FILENUMBER;
    Z11_I2 = Z11_I1+SOLUTIONNUMBER-1;

    Z12_R1 = Z11_I1+SOLUTIONNUMBER*FILENUMBER;
    Z12_R2 = Z12_R1+SOLUTIONNUMBER-1;
    Z12_I1 = Z12_R1+SOLUTIONNUMBER*FILENUMBER;
    Z12_I2 = Z12_I1+SOLUTIONNUMBER-1;

    Z21_R1 = Z12_I1+SOLUTIONNUMBER*FILENUMBER;
    Z21_R2 = Z21_R1+SOLUTIONNUMBER-1;
    Z21_I1 = Z21_R1+SOLUTIONNUMBER*FILENUMBER;
    Z21_I2 = Z21_I1+SOLUTIONNUMBER-1;

    Z22_R1 = Z21_I1+SOLUTIONNUMBER*FILENUMBER;
    Z22_R2 = Z22_R1+SOLUTIONNUMBER-1;
    Z22_I1 = Z22_R1+SOLUTIONNUMBER*FILENUMBER;
```

```

Z22_I2 = Z22_I1+SOLUTIONNUMBER-1;

ZDATA(:, :, i) = [DATA(:, 1) DATA(:, Z11_R1:Z11_R2) DATA(:, Z11_I1:Z11_I2)
DATA(:, Z12_R1:Z12_R2) DATA(:, Z12_I1:Z12_I2)...
DATA(:, Z21_R1:Z21_R2) DATA(:, Z21_I1:Z21_I2)
DATA(:, Z22_R1:Z22_R2) DATA(:, Z22_I1:Z22_I2)];
end

for i = 1:FILENUMBER

    for j = 1:SOLUTIONNUMBER          % Z11 Real
        for k = 1:MAXPASSES
            if isnan(ZDATA(k, j+1+SOLUTIONNUMBER*0, i)) == 1
                Z11(j, i) = Z11(j, i) + ZDATA(k-1, j+1+SOLUTIONNUMBER*0, i);
                break;
            elseif k == MAXPASSES
                Z11(j, i) = Z11(j, i) + ZDATA(k, j+1+SOLUTIONNUMBER*0, i);
            end
        end
    end

    for j = 1:SOLUTIONNUMBER          % Z11 Imaginary
        for k = 1:MAXPASSES
            if isnan(ZDATA(k, j+1+SOLUTIONNUMBER*1, i)) == 1
                Z11(j, i) = Z11(j, i) + ZDATA(k-1, j+1+SOLUTIONNUMBER*1, i)*1i;
                break;
            elseif k == MAXPASSES
                Z11(j, i) = Z11(j, i) + ZDATA(k, j+1+SOLUTIONNUMBER*1, i)*1i;
            end
        end
    end

    for j = 1:SOLUTIONNUMBER          % Z12 Real
        for k = 1:MAXPASSES
            if isnan(ZDATA(k, j+1+SOLUTIONNUMBER*2, i)) == 1
                Z12(j, i) = Z12(j, i) + ZDATA(k-1, j+1+SOLUTIONNUMBER*2, i);
                break;
            elseif k == MAXPASSES
                Z12(j, i) = Z12(j, i) + ZDATA(k, j+1+SOLUTIONNUMBER*2, i);
            end
        end
    end

    for j = 1:SOLUTIONNUMBER          % Z12 Imaginary
        for k = 1:MAXPASSES
            if isnan(ZDATA(k, j+1+SOLUTIONNUMBER*3, i)) == 1
                Z12(j, i) = Z12(j, i) + ZDATA(k-1, j+1+SOLUTIONNUMBER*3, i)*1i;
                break;
            elseif k == MAXPASSES
                Z12(j, i) = Z12(j, i) + ZDATA(k, j+1+SOLUTIONNUMBER*3, i)*1i;
            end
        end
    end

    for j = 1:SOLUTIONNUMBER          % Z22 Real

```

```

    for k = 1:MAXPASSES
        if isnan(ZDATA(k,j+1+SOLUTIONNUMBER*6,i)) == 1
            Z22(j,i) = Z22(j,i) + ZDATA(k-1,j+1+SOLUTIONNUMBER*6,i);
            break;
        elseif k == MAXPASSES
            Z22(j,i) = Z22(j,i) + ZDATA(k,j+1+SOLUTIONNUMBER*6,i);
        end
    end
end

for j = 1:SOLUTIONNUMBER          % Z22 Imaginary
    for k = 1:MAXPASSES
        if isnan(ZDATA(k,j+1+SOLUTIONNUMBER*7,i)) == 1
            Z22(j,i) = Z22(j,i) + ZDATA(k-1,j+1+SOLUTIONNUMBER*7,i)*1i;
            break;
        elseif k == MAXPASSES
            Z22(j,i) = Z22(j,i) + ZDATA(k,j+1+SOLUTIONNUMBER*7,i)*1i;
        end
    end
end

end

VD = zeros(FILENUMBER,SOLUTIONNUMBER);
ID = zeros(FILENUMBER,SOLUTIONNUMBER);
PD = zeros(FILENUMBER,SOLUTIONNUMBER);
Vs = VD;
PDdB = PD;

for i = 1:FILENUMBER
    for j = 1:SOLUTIONNUMBER
        Vs(i,j) = sqrt(POUT/real(Z11(j,i)))*Z11(j,i);
        VD(i,j) = (Z12(j,i)/Z11(j,i))*abs(Vs(i,j));
        ID(i,j) = (Z12(j,i)/(Z12(j,i)*Z12(j,i)-
Z11(j,i)*Z22(j,i)))*abs(Vs(i,j));
        PD(i,j) = abs(VD(i,j)*ID(i,j));
        PDDb(i,j) = 10*log10(abs(VD(i,j)*ID(i,j)))+30;
    end
end

W = 10:5:30;
H = 2:2:10;
[xp,yp] = meshgrid(W,H);
for i = 1:length(H)
    zp(i,:) = PDDb(1,1+length(W)*(i-1):length(W)*i);
end

figure (1)
mesh(xp,yp,zp);
figure (2)
for i=1:5
    plot(xp(i,:),zp(i,:));
    hold on;
end
hold off;

```

## APPENDIX G

### MATLAB CODE FOR PLOTTING TAG ANGLE VS POWER

```
% This program plots the efficiency vs touch probe placement

% HF
theta = [-pi -5*pi/6 -4*pi/6 -3*pi/6 -2*pi/6 -pi/6 0 pi/6 2*pi/6 3*pi/6
4*pi/6 5*pi/6 pi];
rho = [-40 0 40];
[t r] = meshgrid(theta, rho);
p = [25.2 19.8 10.2 0.44 10.2 19.8 25.2 19.8 10.2 0.44 10.2 19.8 25.2;
      100 84.5 46.9 1.17 46.9 84.5 100 84.5 46.9 1.17 46.9 84.5 100;
      25.2 19.8 10.2 0.44 10.2 19.8 25.2 19.8 10.2 0.44 10.2 19.8 25.2];

% define parameter in polar coordinates
thetaI = -pi:pi/72:pi;
rhoI = -40:0.5:40;
[tI rI] = meshgrid(thetaI, rhoI);

pI = interp2(t,r,p,tI,rI); % data interpolation

% conversion from polar coordinates to Cartesian
[xp yp] = pol2cart(tI,rI);
zp = pI;

figure(1)
surf(xp,yp,zp);
grid off

% UHF
theta = [-pi -5*pi/6 -4*pi/6 -3*pi/6 -2*pi/6 -pi/6 0 pi/6 2*pi/6 3*pi/6
4*pi/6 5*pi/6 pi];
rho = [-40 0 40];
[t r] = meshgrid(theta, rho);
p = [21.5 10.0 0.80 0.54 0.80 10.0 21.5 10.0 0.80 0.54 0.80 10.0 21.5;
      100 87.8 51.4 3.40 51.4 87.8 100 87.8 51.4 3.40 51.4 87.8 100;
      21.5 10.0 0.80 0.54 0.80 10.0 21.5 10.0 0.80 0.54 0.80 10.0 21.5];
```

```
% define parameter in polar coordinates
thetaI = -pi:pi/72:pi;
rhoI = -40:0.5:40;
[tI rI] = meshgrid(thetaI, rhoI);

pI = interp2(t,r,p,tI,rI); % data interpolation

% conversion from polar coordinates to Cartesian
[xp yp] = pol2cart(tI,rI);
zp = pI;

figure(2)
surf(xp,yp,zp);
grid off
```

## BIBLIOGRAPHY

- [1] K. J. Hamelynck. The history of mobile-bearing total knee replacement systems. *Orthopedics*, 29 (9 Suppl): S7–12, 2006.
- [2] S. Almouahed, M. Gouriou, C. Hamitouche, E. Stindel, and C. Roux. Design and evaluation of instrumented smart knee implant. *IEEE Trans. Biomed. Engr.*, 58(4), Apr 2011.
- [3] X. Liu, A. Ogirala, L. Berger and M. H. Mickle. Design and implementation of a volume conduction based RFID system for smart implants. *IEEE EMBS'11*, Aug 2011.
- [4] R. Weinstein. RFID: a technical overview and its application to the enterprise. *IT professional*, 7(3): 27-33, May-June 2005.
- [5] Bloomberg business week report.  
[http://www.businessweek.com/technology/content/aug2005/tc2005089\\_4131\\_tc\\_215.htm](http://www.businessweek.com/technology/content/aug2005/tc2005089_4131_tc_215.htm)
- [6] Clearcount smart sponge system. <http://clearcount.com/products/smart sponge-system>
- [7] S. Kurtz. Total knee and hip replacement surgery projections show meteoric rise by 2030. Orthopaedic procedures set to continue gaining widespread acceptance as means to restore quality-of-life. *Annual Meeting of the AAOS'06*, March 2006.
- [8] N. A. Wilson, E. S. Schneller, K. Montgomery and K. J. Bozic. Hip and knee implants: current trends and policy considerations. *Health Aff (Millwood)* (27):1587-1598, 2008.
- [9] Freedomia Group. Orthopedic implants to 2012 - market research, market share, market size, sales, demand forecast, market leaders, company profiles, industry trends. URL: <http://www.freedoniagroup.com/Orthopedic-Implants.html>.
- [10] J. Bellemans, M. Ries and J. Victor. *Total Knee Arthroplasty: A Guide to Get Better Performance*. Springer, 2005
- [11] S.M. Kurtz, K. Ong, E. Lau, F. Mowat, M. Halpern. Projections of primary and revision hip and knee arthroplasty in the United States from 2005 to 2030. *J. Bone Joint Surg. Am.*, 89(4):780-785, 2007

- [12] Radio frequency identification.  
URL: [http://en.wikipedia.org/wiki/Radio-frequency\\_identification](http://en.wikipedia.org/wiki/Radio-frequency_identification).
- [13] K. Finkenzeller. *RFID Handbook: Fundamentals and Applications in Contactless Smart Cards, Radio Frequency Identification and Near-field Communication*. Wiley, 2003.
- [14] Y. Hwang and H. Lin. A new CMOS analog front end for RFID tags. *IEEE Trans. Industrial Electronics*, 56(7): 2299-2307, 2009
- [15] TegoChip. URL: [http://www.tegoinc.com/products/products\\_tegochip.php](http://www.tegoinc.com/products/products_tegochip.php).
- [16] M. A. Hughes and R. M. Pratt. Semi-passive radio frequency identification (RFID) tag with active beacon. U. S. Patent No. 7,348,875, Mar 2008.
- [17] J. D. Porter and D. S. Kim. An RFID-enabled road pricing system for transportation. *IEEE Systems J.*, 2(20), Jun 2008.
- [18] W. Pentland and D. E. Gumpert. USDA bets the farm on animal ID program. *The Nation*, Dec 31, 2007.
- [19] P. Potter, B. Daskala and R. Compano. RFID implants: opportunities and challenges for identifying people. *IEEE Technology and Society Magazine*, 27, 2008.
- [20] Verichip. URL: <http://en.wikipedia.org/wiki/VeriChip>.
- [21] J. Proakis and M. Salehi. *Digital communications*. McGraw-Hill, 2007.
- [22] ISO/IEC FDIS 18000-3: RFID for item management-Air interface, Part 3 - Parameters for air interface communications at 13.56 MHz, April 2003.
- [23] R. S. Mackay. *Bio-medical Telemetry: Sensing and Transmitting Biological Information from Animals and Man*. Wiley, New York, 2nd edition, 1998.
- [24] J. Banks. Past, present and future of RFID. *IEEE Intl. Conf. Automation and Logistics*, pp. 26-27, Aug 2007.
- [25] Information technology automatic identification and data capture technique - Radio frequency identification for item management air interface - Part 6: Parameters for air interface communications at 860–960 MHz. ISO/IEC FDIS 1800-6, Nov 2003.
- [26] P. Foster and R. Burberry. Antenna problems in RFID systems. In *Inst. Elect. Eng. Colloquium on RFID Technology*, 31–35, 1999.
- [27] D. Dobkin. and S. Weigand. Environmental effects on RFID tag antennas. *IEEE MTT-S International Microwave Symposium Digest*, 135-138, 2005.
- [28] X. Qing and Z. Chen. Proximity effects of metallic environments on high frequency RFID reader antenna: study and applications. *IEEE Trans. Antennas and Propagation*, 55, Nov 2007.

- [29] X. Qing and Z. Chen. Characteristics of a metal-backed loop antenna and its application to a high-frequency RFID smart shelf. *IEEE Antennas and Propagation Magazine*, 51(2): 26-38, 2009
- [30] J. Griffin and G. Durgin. Gains for RF tags using multiple antennas. *IEEE Trans. Antennas and Propagation*, 56(2): 563-570, Feb 2008.
- [31] A. Ogirala, M. H. Mickle, J. R. Stachel, D. Rong, P. J. Hawrylak, R. K. Yalamanchili, M.I A. Rothfuss, and X. Liu. Impact of ISO 18000 series RF signals on CRMDs: a unified approach. *International Journal of Modelling and Simulation*, 31, 2011.
- [32] B. Nouredine, M. Mohamed and K. Smain. Attenuation in transferred RF power to a biomedical implant due to the absorption of biological tissue. *World Academy of Science, Engineering and Technology*. 10, pp. 165-168, 2005.
- [33] D. Werber, A. Schwentner and E.M. Biebl. Investigation of RF transmission properties of human tissues. *Adv. Radio Sci.*, 4: 357-360, 2006
- [34] D. Lindsey, E. McKee, M. Hull, and S. Howell. A new technique for transmission of signals from implantable transducers. *IEEE Trans. Biomed. Engr.*, 45: 614-619, 1998.
- [35] E. L. McKee, D. P. Lindsey, M. L. Hull, and S. M. Howell. Telemetry system for monitoring anterior cruciate ligament graft forces in vivo. *Med. Biol. Eng. Comput.*, 36, 1998.
- [36] L. Williams, W. Vablais and S. Bathiche. Method and apparatus for transmitting power and data using the human body. U. S. Patent No. 6,754,472, Jun 2004.
- [37] N. M. Neihart and R. R. Harrison. A low-power fm transmitter for use in neural recording applications. *IEEE EMBS'04*, 2117-2120, 2004.
- [38] S. A. Hackworth, M. Sun and R. J. Sclabassi. A prototype volume conduction platform for implantable devices. *IEEE NEBEC*, Mar 2007.
- [39] S. A. Hackworth. Design, optimization, and implementation of a volume conduction energy transfer platform for implantable devices. Doctoral dissertation, University of Pittsburgh, 2010
- [40] K. W. Horch and G. S. Dhillon. *Neuroprosthetics: Theory and Practice*. World Scientific, River Edge, NJ, 2004.
- [41] G. Matthaei, E. M. T. Jones and L. Young. Microwave filters, impedance-matching networks, and coupling structures. *Artech House*, Feb 1980.
- [42] C. Choo and H. Ling. Design of electrically small planar antennas using inductively coupled feed. *Electron. Lett.*, 39:1563-1565, Oct 2003.

- [43] H. Choo and H. Ling. Electrically small planar antennas with inductively coupled feed. US patent 7,061,440, Jun 2006.
- [44] J. Choo, J. Ryoo, J. Hong, H. Jeon, C. Choi and M. M. Tentzer. T-matching networks for the efficient matching of practical RFID Tags. *EuMC'09*, 2009.
- [45] G. Marrocco. The art of UHF RFID antenna design: impedance-matching and size-reduction techniques. *IEEE Antenna and Propagation Magazine*, 50(1), Feb 2008.
- [46] W. A. Davis and K. Agarwal. *Radio frequency circuit design*. Wiley, 2001.
- [47] Impedance matching. [http://en.wikipedia.org/wiki/Impedance\\_matching](http://en.wikipedia.org/wiki/Impedance_matching)
- [48] J. Mingo, A. Valdovinos, D. Navarro and P. Garcia. An RF electronically controlled impedance tuning network design and its application to an antenna input impedance automatic matching system. *IEEE Trans. Microwave Theory and Techniques*, 52(2): 489-497, 2004.
- [49] American National Standard. ANSI/AAMI PC-69:2007 Active implantable medical devices-Electromagnetic compatibility-EMC test protocols for implantable cardiac pacemakers and implantable cardioverter defibrillators, 2007.
- [50] Y. Wang, H. Sha, S. Zhao and C. Ren. Optimizing of electrode system with central object in electrical impedance tomography. *Inst. Of Biomed. Eng.*, 2009
- [51] IEEE standard for safety levels with respect to human exposure to radio frequency electromagnetic fields, 3 khz to 300 ghz. Technical Report C95.1, IEEE, New York, NY, Apr 2006. Sponsor: IEEE International Committee on Electromagnetic Safety (SCC39).
- [52] G. Marrocco. Gain-optimized self-resonant meander line antennas for RFID applications. *IEEE Antennas and Wireless Propagation Letters*, 2: 302-305, 2003.
- [53] D. Ratner, A. S. Hoffman, F. J. Schoen, and J. E. Lemons. *Biomaterials Science: An Introduction to Materials in Medicine*. Elsevier Academic Press, San Diego, CA, 2nd edition, 2004.
- [54] G. E. Loeb, R. A. Peck, and J. Martyniuk. Toward the ultimate metal microelectrode. *J. Neurosci. Meth.*, 63:175-183, 1995.
- [55] J. D. Weiland, D. J. Anderson, and M. S. Humayun. In vitro electrical properties for iridium oxide versus titanium nitride stimulating electrodes. *IEEE Trans. Biomed. Engr.*, 49(12):1574-1579, Dec 2002.
- [56] Magellan Technology. *Magellan Reader Manager Guide v2.05*, 2008
- [57] M. J. Donahoo and K. L. Calvert. *TCP/IP Sockets in C Bundle: TCP/IP Sockets in C, Second Edition: Practical Guide for Programmers*. Morgan Kaufmann, 2009

- [58] Magellan Technology. *Magellan Reader Application Programmer's Guide for Readerserver 3.30*, 2008.
- [59] ANSYS/HFSS. URL: <http://www.ansoft.com/products/hf/hfss>.
- [60] An Internet resource for the calculation of the dielectric properties of body tissues in the frequency range 10 Hz - 100 GHz. URL: <http://niremf.ifac.cnr.it/tissprop>.
- [61] A. F. Coston and J. K-J. Li. Transdermal drug delivery: a comparative analysis of skin impedance models and parameters. *IEEE EMBS '03*, 2982-2985, Sep 2003.
- [62] Z. Tang, R. J. Scwabassi, C. Sun, S. A. Hackworth, J. Zhao, X. T. Cui and M. Sun. Transcutaneous battery recharging by volume conduction and its circuit modeling. *IEEE EMBS*, 644-647, 2006
- [63] J. Malmivuo and R. Plonsey. Bioelectromagnetism: Principles and Applications of Bioelectric and Biomagnetic Fields. *Oxford University Press*, 1995
- [64] D. Misra. Radio-frequency and microwave communication circuits: analysis and design. *Wiley*, 2002.
- [65] P. Moin. Fundamentals of engineering numerical analysis. *Cambridge University Press*, 2001.
- [66] D. Panescu, J. G. Webster and R. A. Stratbucker. A nonlinear electrical-thermal model of the skin. *IEEE Trans. Biomed. Eng.*, 41(7):672-80, Jul 1994.
- [67] A. Kimoto and K. Shida. Imaging of temperature-change distribution in the brain phantom by means of capacitance measurement. *IEEE Trans. on Instrumentation and Measurement*, 49(3): 591-595, Jun 2000.
- [68] J. Conway. Electrical impedance tomography for thermal monitoring of hyperthermia treatment: an assessment using in vitro and in vivo measurements. *Clin. Phys. Physiol. Meas.*, 8(Suppl): 141-6, 1987.
- [69] E. Husain and S. M. Islam. Effect of electrode shape, material and chemical structure on electric strength of some liquid hydrocarbons. *Intl. Conf. Conduction and Breakdown in Dielectric Liquids*, 1990.
- [70] S. Shah, A. Chu, D. Zhou, R. Greenberg, D. Guven, M. S. Humayun and J. D. Weiland. Intraocular impedance as a function of the position in the eye, electrode material and electrode size. *IEEE EMBS'04*, Sep 2004
- [71] AAPL. *The AAPL handbook for Radio Communications: the Comprehensive RF Engineering Reference*, 2011
- [72] ANSYS, Inc. Ansoft HFSS User Guide, 2009.